A SELF-CONTAINED, AUTOMATED METHODOLOGY FOR OPTIMAL FLOW CONTROL VALIDATED FOR TRANSITION DELAY

Ronald D. Joslin,[1] Max D. Gunzburger,[2] R. A. Nicolaides,[3]
Gordon Erlebacher,[4] and M. Yousuff Hussaini[4]

[1] *NASA Langley Research Center, Hampton VA 23681-0001*
[2] *Virginia Polytechnic Institute and State University, Blacksburg VA 24061-0531*
[3] *Carnegie Mellon University, Pittsburgh PA 15213*
[4] *ICASE, NASA Langley Research Center, Hampton VA 23681-0001*

Abstract

This paper describes a self-contained, automated methodology for flow control along with a validation of the methodology for the problem of boundary layer instability suppression. The objective of control is to match the stress vector along a portion of the boundary to a given vector; instability suppression is achieved by choosing the given vector to be that of a steady base flow, e.g., Blasius boundary layer. Control is effected through the injection or suction of fluid through a single orifice on the boundary. The present approach couples the time-dependent Navier-Stokes system with an adjoint Navier-Stokes system and optimality conditions from which optimal states, i.e., unsteady flow fields, and controls, e.g., actuators, may be determined. The results demonstrate that instability suppression can be achieved without any a priori knowledge of the disturbance, which is significant because other control techniques have required some knowledge of the flow unsteadiness such as frequencies, instability type, etc.

[1] This research was supported by the National Aeronautics and Space Administration under NASA Contract No. NAS1-19480 while the authors (except the first) were in residence at the Institute for Computer Applications in Science and Engineering (ICASE), NASA Langley Research Center, Hampton, VA 23681.

1. INTRODUCTION

In the last decade, increasing attention has been devoted to the development of techniques capable of enhancing our ability to control the unsteady flow in a wide variety of configurations such as engine inlets and nozzles, combustors, automobiles, aircraft, and marine vehicles. Controlling the flow in these configurations can lead to greatly improved efficiency and performance, while decreasing the noise levels generally associated with the otherwise unattended unsteady flow. Depending on the desired result, one might wish to delay *or* accelerate transition, reduce drag *or* or enhance mixing. There might be a need to postpone flow-separation, increase lift or manipulate a turbulence field. Gad-el-Hak (1989) and Gad-el-Hak & Bushnell (1991) provide an excellent introduction to and overview of various control methodologies.

Small improvements in system performance often lead to large payoffs. For example, Butter (1984) estimates that a 5 percent improvement in landing maximum lift coefficient ($C_l(\max)$) can translate to a 25 percent increase in payload, while a 12 to 15 percent payload increase could result from only a 5 percent improvement in the takeoff $C_l(\max)$. As further evidence of the gains of a well-controlled system, Cousteix (1992) notes that 45 percent of the drag for a commercial transport transonic aircraft is due to skin friction on the wings, fuselage, fin, etc., and that a 10 to 15 percent reduction of the total drag can be expected simply by laminarizing the flow over the wings and the fin. This translates into a reduction in fuel requirements, improved performance, and/or increased payload. Muirhead (1978) has shown with a wind tunnel investigation that control of flow separation on a tractor-trailor truck can reduce the drag by 30 to 40 percent of the baseline truck configuration. This translates into a savings of millions of barrels of oil per year.

Encouraged by the potential for huge rewards with what seems to be a rather modest input, research into ways of achieving the above gains is attaining increasing importance. In many technologically important situations, the flow usually starts from a smooth laminar state which is inherently unstable and develops instability waves downstream. These instability waves grow expoenentially entailing nonlinear interactions, which lead ultimately to full developed turbulence. This process is present in various forms in most systems. Therefore, one goal of a good control system is to inhibit strongly, if not eliminate altogether, the instabilities which lead to an undesirable transitional or turbulent state.

1.1 The Wave-Cancellation Concept

The simplest form of control which might achieve this objective is the wave-cancellation approach, based on the premise (mostly correct) that the instability mechanisms in a low-speed transition are crucially dominated by a single two-dimensional instability wave; therefore, cancelling this wave will preclude the nonlinear interactions leading to laminar-turbulent transition. The wave-cancellation method further assumes that a wavelike disturbance can be linearly cancelled by introducing another wave equal in amplitude but opposite in phase, and thus it is mostly applicable to systems governed by linear or quasi-linear equations. The key is to determine the parameters of the downstream wave which counter (cancel) the evolution of the upstream generated wave. Although there is little theoretical work on this topic, there are a number of experiments and numerical simulations which validate this approach. Both passive and active forms of control are possible, and an active control might or might not make use of feedback. Passive control makes use of gemetrical and physical characteristics to affect the flow. There is no wave-dependent input by an external device which might require energetic input. In the passive case without feedback, one inputs a wave with the proper phase and amplitude downstream of the source (actuator), using knowledge of the upstream input. Better and more robust results can be achieved via active control with feedback. This technique identifies the characteristics of the wave downstream of the actuator using a sensor, and feeds back (time-dependent) information to the actuator. Different types of controls, all leading to different levels of wave-cancellation have been studied, both experimentally and numerically. The aim is of course to achieve the perfect cancellation, wherein the input wave has the same shape as the input wave at one or several locations on the body, and exactly π radians out of phase. Of course, this is not achievable in practice, as system imperfections and nonlinearities prevent perfect wave cancellation.

Most of the experiments, aimed at verifying the wave-cancellation concept, were conducted on the flat plate, except those of Ladd & Hendricks (1988), Pupator & Saric (1989), and Ladd (1990), who considered axisymmetric bodies. Many of these experiments were conducted in water tunnels. Vibrating wires (Milling 1981), hot strips (Liepmann & Nosenchuck 1982a,b), suction and blowing (Pupator & Saric 1989; Ladd 1990), electromagnetic generators (Thomas 1983), and adaptive heating (Ladd & Hendricks 1988), are some of the methods that were used to generate the controlling wave. All these input mechanisms give the experimenter control over the phase and amplitude of the input wave. The experimentalists met with varying degrees of success. Among the more successful studies

were those of Milling (1981) and Thomas (1983) who achieved at least an 80 percent reduction in the input amplitude of the 2-D wave (with 0.6%-1% amplitude). However, it was not possible to achieve relaminarization, probably because of the three-dimensionality of the flow resulting from the interaction between background disturbances and the primary 2-D wave. As expected, the studies conducted on axisymmetric bodies produced relatively less wave-cancellation since these flows are highly three-dimensional. Furthermore, good wave-cancellation results requires a linear system with constant coefficients. This requirement is clearly violated for a flow over a body with curvature.

In addition to the aforementioned experiments, several theoretical (i.e., linear computations and theory) and computational studies (i.e, nonlinear simulations) have focused on understanding the physics of this wave-cancellation process. Maestrello & Ting (1984) provided a linear asymptotic analysis to demonstrate the relationship between the input of localized disturbances and their effect on the Tollmien-Schlichting (TS) instability waves present in the wall-bounded shear flow. They showed that small amounts of local periodic heating could excite disturbances that actively control the TS waves which propagate in a boundary layer on a flat plate. Analogous to the experiments, several wave input mechanisms were considered. In one of the early Navier-Stokes simulations of active control, Biringen (1984) used suction and blowing at the wall in a channel flow. He observed approximately a 50 percent reduction in the amplitudes of the 2-D instabilities and a decrease in the growth of the 3-D instabilities. The Reynolds stress originally generated by the waves was all but removed. On the other hand, Metcalfe, Rutland, Duncan & Riley (1985) studied the effect of a moving wall on unstable waves traveling in a laminar flow on a flat plate. The simulations were based on the Navier-Stokes equations solved within a temporal framework. An energy analysis revealed that the wall motion causes the Reynolds-stress term to become negative, which implies a feed of energy from the perturbed flow back into the mean flow. In effect, this energy analysis showed how a perturbation to an unstable flow can be stabilizing. However, an instability wave eventually formed downstream of the control, with the same growth rate as the uncontrolled wave. This is a clear indication that the cancellation was not complete. Although intuitively obvious, until the work of Bower, Kegelman, Pal & Meyer (1987) and Pal, Bower & Meyer (1991), it was not known that perfect cancellation could be obtained within the context of linear theory (for which the mean flow is independent of the propagating direction. They used the 2-D Orr-Sommerfeld equation to study and control instability-wave growth by superposition, and showed, within the limits of linear stability theory and the parallel-flow

assumption, that single and multifrequency waves can be cancelled. The basic conclusions drawn by the early experimentalists were confirmed by the studies of Laurien & Kleiser (1989) and Kral & Fasel (1989). They showed that it was possible to delay or accelerate (but not eliminate) transition by appropriately (either by heating or by suction and blowing) superposing disturbances out of (in) phase with the primary TS wave. To get the best results required that the control be applied in the linear stages of transition, before the secondary instability sets in. Similar results were also reported by Danabasoglu, Biringen & Street (1991).

All of the previous active-control studies were undertaken with the *a priori* assumption that wave cancellation was accomplished by the linear superposition (or forcing) of waves with π radian phase shifts, or one-half wavelength/period phase shifts. None of these previous studies were able to achieve complete (or exact) instability removal (wave cancellation) from the flow, except for the linear studies reported by Milling (1981) and Pal, Bower & Meyer (1991), where the limitations of hydrodynamic linear instability theory were assumed. In practice, complete cancellation is not possible with a single actuator because any small residual of the cancelled wave will grow exponentially with downstream distance. Therefore, the wave will reappear some small distance downstream.

Although there have been quite a few studies on the so-called wave-cancellation approach, no effort was made to demonstrate clearly that wave cancellation was in fact responsible for the observed reduction in wave amplitude. Recently, Joslin, Erlebacher & Hussaini (1995) performed a numerical experiment which served to unequivocally demonstrate the link between linear superposition and instability suppression. To ensure that linear superposition of individual instabilities was, in fact, responsible for the results found in previous experiments and computations, they carried out three simulations with i) only the disturbance; ii) only the control; and iii) using both disturbance and control, which is the wave-cancellation case. By discretely summing the control-only and forcing-only numerical results, they found that this linear superposed solution is identical to the wave-cancellation results. These tests cleary verify the hypothesis that linear superposition is the reason for the previous experimental and computational results.

From the above experiments, linear computations and nonlinear simulations, several common features emerge: i) It is impossible to achieve perfect wave cancellation unless the system is linear, with constant coefficients; ii) the efficiency of wave cancellation decreases as the system becomes more nonlinear; iii) as the geometry of the configuration becomes more complex, cancellation becomes more difficult; and iv) the current approaches require

foreknowledge of the instability wave characteristics, such as its frequency and amplitude.

1.2 Optimal Control Theory

The optimal control theory provides an approach which does not require a priori knowledge of the flow characteristics. The goal of optimal control theory is indeed to minimize or maximize an objective function in a robust manner. When the flow is time-dependent, and a strong function of initial conditions, it becomes difficult to establish the precise controls that will achieve the desired effect. Wave-cancellation, as discussed above, only works well when the input wave has a dominant frequency, and its properties are known. Then (either in a passive fashion, or through a feedback mechanism), one seeks to cancel its effect while still in a linear regime. In practice, there are many waves, which can interact nonlinearly in ways not always known in advance. Rather than try to cancel the incoming waves, one seeks appropriate controls in other ways. One means of achieving this, without an extensive search over the space of possible controls, is to postulate a family of desired controls (e.g., an arbitrary time-dependent amplitude and a specified spatial distribution), and an objective function (i.e., stress over a region of the plate). Then, through a formal minimization process, one derives a set of differential equations, and their adjoints, whose solution produces the optimal actuator profile (among the specified set). While the solution to this set of equations cannot be accomplished in real time, the results can be applied using standard passive or active control mechanisms. The advantage is that entire collections of controls can be studied simultaneously, rather than one at a time.

Optimal control methodologies have been recently applied to a variety of problems involving drag reduction, flow and temperature matching, etc. to provide more sophisticated flow control strategies in engineering applications. This is possible because computational fluid dynamics (CFD) algorithms have reached a sufficiently high level of maturity, generality, and efficiency so that it is now feasible to implement sophisticated flow optimization methods, which lead to a large number of coupled partial differential equations. Optimal control theory is quite mathematical, and its formal nature is amenable to the derivation of mathematical theorems related to existence of solutions and well-posedness of the problem. Two recent surveys of the mathematical theories of optimal flow control are Gunzburger (1995) and Borggaard et al. (1995). For a mathematical treatment of a problem very similar to the one considered in this paper, one may consult Fursikov, Gunzburger & Hou (1995). Optimal control techniques will not provide the real time control that one is ultimately interested in, but by systematically computing the best control within specified

tolerances, with a given objective function, it will be possible to develop strategies (active or passive) to control a wide variety of disturbances). For example, to effectively control a boundary-layer transition due to the interaction of cross-flow and TS wave using periodic heating and cooling, optimal control would allow: 1) a determination of the best objective function to use for a given type of control (some are better than others), and 2) provide insight into the relationship between the time dependence of the control and the input waves. This insight could then be built into a neural network, or other type of self-learning system, to allow effective control over a wide range of input parameters.

1.3 The Current Approach

The methodology of the current paper is based on defining a control mechanism and an objective for control, and then finding, in a systematic and automated manner, controls that best meet the objecive. In the present setting, an objective or cost functional is defined that measures the "distance" between the measured stresses, and their desired values along a limited section of the bounding wall and over a specified length of time. One may interpret the objective functional as a "sensor," i.e., the objective functional senses how far the flow stresses along the wall are from the corresponding desired values. To control the flow, we imposed time-dependent injection and suction along a small orifice in the bounding wall. Although the spatial dependence of the suction profile is specified (for simplicity), the optimal control methodology determines the time-variation of this profile. However, unlike feedback control methodologies wherein the sensed data determines the control through a specified feedback law or controller, here the time-dependence of the control is the natural result of the minimization of the objective functional. This scenario is shown in Figure 1. We have a sensor that feeds information to a controller that in turn feeds information to the actuator. However, in the optimal control setting, the sensor is actually an objective functional and the controller is a coupled system of partial differential equations that determine the control that does the best job of minimizing the objective functional. The present active-control approach is demonstrated for the evolution and automated control of of spatially growing 2D disturbances in a flat-plate boundary layer. As the length of time over which the minimization process is increased, we recover the results obtained by wave cancellation, thus validating the approach. The ultimate goal of this line of research is to introduce automated control to external flows over realistic configurations such as wings and fuselages, and to devise novel flow control techniques.

2. THE OPTIMIZATION PROBLEM

2.1. The state equations

Let Ω denote the flow domain which is the semi-infinite channel or boundary layer $[x \geq 0,\ 0 \leq y \leq h]$, where h is the location of the upper wall for the channel or the truncated freestream distance for the boundary layer. Let Γ denote its boundary and let $(0,T)$ be the time interval of interest. The inflow part of the boundary $[x = 0, 0 \leq y \leq h]$ is denoted by Γ_i and the part of the boundary on which control is applied (i.e., along which the suction and blowing actuator is placed) by Γ_a which is assumed to be a finite connected part of the lower boundary (or wall) $[x \geq 0,\ y = 0]$. Solid walls are denoted by Γ_w; for the channel flow, Γ_w is the lower boundary $[x \geq 0,\ y = 0]$ with Γ_a excluded and the upper boundary $[x \geq 0,\ y = h]$; for the boundary layer flow, Γ_w is only the lower boundary with Γ_a excluded. For the boundary-layer case, the upper boundary $[x \geq 0,\ y = h]$, which is not part of Γ_w, is denoted by Γ_e. Controls are only activated over the given time interval $t \in (T_0, T_1)$, where $0 \leq T_0 < T_1 \leq T$.

The flow field is described by the velocity vector (u, v) and the scalar pressure p and is obtained by solving the following momentum and mass conservation equations

$$\frac{\partial u}{\partial t} + u\frac{\partial u}{\partial x} + v\frac{\partial u}{\partial y} + \frac{\partial p}{\partial x} - \nu\frac{\partial}{\partial x}\left(2\frac{\partial u}{\partial x}\right) - \nu\frac{\partial}{\partial y}\left(\frac{\partial u}{\partial y} + \frac{\partial v}{\partial x}\right) = 0 \quad \text{in } (0,T)\times\Omega\,, \tag{1}$$

$$\frac{\partial v}{\partial t} + u\frac{\partial v}{\partial x} + v\frac{\partial v}{\partial y} + \frac{\partial p}{\partial y} - \nu\frac{\partial}{\partial x}\left(\frac{\partial u}{\partial y} + \frac{\partial v}{\partial x}\right) - \nu\frac{\partial}{\partial y}\left(2\frac{\partial v}{\partial y}\right) = 0 \quad \text{in } (0,T)\times\Omega\,, \tag{2}$$

$$\frac{\partial u}{\partial x} + \frac{\partial v}{\partial y} = 0 \quad \text{in } (0,T)\times\Omega\,, \tag{3}$$

subject to initial and boundary conditions:

$$\left.\begin{pmatrix} u \\ v \end{pmatrix}\right|_{t=0} = \begin{pmatrix} u_0 \\ v_0 \end{pmatrix} \quad \text{in } \Omega\,, \tag{4}$$

$$\left.\begin{pmatrix} u \\ v \end{pmatrix}\right|_{\Gamma_a} = \begin{cases} \begin{pmatrix} g_1 \\ g_2 \end{pmatrix} & \text{in } (T_0, T_1) \\ \begin{pmatrix} 0 \\ 0 \end{pmatrix} & \text{in } (0,T_0) \text{ and } (T_1,T)\,, \end{cases} \tag{5}$$

$$\left.\begin{pmatrix} u \\ v \end{pmatrix}\right|_{\Gamma_i} = \begin{pmatrix} u_i \\ v_i \end{pmatrix} \quad \text{in } (0,T)\,, \tag{6}$$

$$\left.\begin{pmatrix} u \\ v \end{pmatrix}\right|_{\Gamma_w} = \begin{pmatrix} 0 \\ 0 \end{pmatrix} \quad \text{in} \quad (0,T)\,, \tag{7}$$

and

$$(u,v,p) \to \text{base flow}, \quad \frac{\partial u}{\partial x} \to 0, \quad \text{and} \quad \frac{\partial v}{\partial x} \to 0 \qquad \text{as} \quad x \to \infty\,. \tag{8}$$

Here, the initial velocity vector $(u_0(x,y), v_0(x,y))$ and the inflow velocity vector $(u_i(t,y), v_i(t,y))$ are assumed given and the base flow is assumed to be Poiseuille flow for the channel case and Blasius flow for the boundary-layer case. The above system holds for both the channel and Blasius flow cases; in the latter case, the upper boundary is not part of Γ_w and the additional boundary condition

$$u|_{\Gamma_e} = U_\infty \qquad \text{and} \qquad \left. p - 2\nu\frac{\partial v}{\partial y}\right|_{\Gamma_e} = P_\infty \qquad \text{in} \quad (0,T) \tag{9}$$

is imposed, where U_∞ and P_∞ denote the free-stream flow speed and pressure, respectively.

The particular form of the viscous terms in (1) and (2) is necessary in order to correctly interpret some boundary integrals that will appear below.

The control functions $g_1(t,x)$ and $g_2(t,x)$ which give the rate at which fluid is injected or sucked tangentially and perpendicularly, respectively, through Γ_a are to be determined as part of the optimization process. In order to make sure that the control remains bounded at T_0, it is required that

$$g_1|_{t=T_0} = g_{10}(x) \quad \text{and} \quad g_2|_{t=T_0} = g_{20}(x) \quad \text{on } \Gamma_a\,, \tag{10}$$

where $g_{10}(x)$ and $g_{20}(x)$ are specified functions defined on Γ_a. Commonly, one chooses $g_{10}(x) = g_{20}(x) = 0$.

2.2. The objective functional and the optimization problem

Assume that Γ_s is a finite, connected part of the lower boundary $[x \geq 0,\, y = 0]$ which is disjoint from Γ_a and that (T_a, T_b) is a time interval such that $0 \leq T_a < T_b \leq T$. Then, consider the functional

$$\begin{aligned} &\mathcal{J}(u,v,p,g_1,g_2) \\ &\quad = \frac{\alpha_1}{2}\int_{T_a}^{T_b}\int_{\Gamma_s}\left|\nu\frac{\partial u}{\partial y} - \tau_1\right|^2 d\Gamma dt + \frac{\alpha_2}{2}\int_{T_a}^{T_b}\int_{\Gamma_s}\left|-p + 2\nu\frac{\partial v}{\partial y} - \tau_2\right|^2 d\Gamma dt \\ &\quad + \frac{\beta_1}{2}\int_{T_0}^{T_1}\int_{\Gamma_a}\Big(\left|\frac{\partial g_1}{\partial t}\right|^2 + |g_1|^2\Big)d\Gamma dt + \frac{\beta_2}{2}\int_{T_0}^{T_1}\int_{\Gamma_a}\Big(\left|\frac{\partial g_2}{\partial t}\right|^2 + |g_2|^2\Big)d\Gamma dt\,, \end{aligned} \tag{11}$$

where g_1 and g_2 denote the controls and $\tau_1(t,x)$ and $\tau_2(t,x)$ are given functions defined on $(T_a,T_b)\times\Gamma_s$. Note that since Γ_s is part of the lower boundary of the channel or boundary-layer wall, $\nu\partial u/\partial y$ and $-p+2\nu\partial v/\partial y$ are the shear and normal stresses, respectively, exerted by the fluid on the bounding wall along Γ_s and thus τ_1 and τ_2 may be interpreted as given shear and normal stresses, repectively. Then, the boundary segment Γ_s can be thought of as a sensor which measures the stresses on the wall. Thus, in (11), Γ_s is the part of the boundary Γ along which one wishes to match the shear and normal stresses to the given functions τ_1 and τ_2, respectively, and (T_a,T_b) is the time interval over which this matching is to take place. (There are no diffilculties, other than notational, introduced if one wishes to match each component of the stress vector over a different boundary segment and/or over a different time interval.)

The third and fourth terms in (11) are used to limit the size of the control. Indeed, no bounds are *a priori* placed on g_1 or g_2; their magnitudes are limited by adding a penalty to the stress matching functional defined by the first two terms in (11). The particular form that these penalty terms take, i.e, the third and fourth terms in (11), is motivated by the necessity to limit not only the size of the controls g_1 and g_2, but also to limit oscillations. The constants α_1, α_2, β_1, and β_2 can be used to adjust the relative importance of the terms appearing in the functional (11).

The (constrained) optimization problem is given as follows:

> *find u,v,p,g_1, and g_2 such that the functional $\mathcal{J}(u,v,p,g_1,g_2)$ given in (11) is minimized subject to the requirement that (1)-(8) and (10) are satisfied and, for the boundary-layer flow case, (9) is also satified.*

3. THE OPTIMALITY SYSTEM

We first consider, in Sections 3.1-3.5, the case of a channel flow; the optimality system for the boundary layer flow is considered in Section 3.6.

3.1. The Lagrangian Functional

The method of Lagrange multipliers is formally used to enforce the constraints (1)-(3)

and (5). To this end, the Lagrangian functional

$$
\begin{aligned}
&\mathcal{L}(u,v,p,g_1,g_2,\hat{u},\hat{v},\hat{p},s_1,s_2)\\
&=\frac{\alpha_1}{2}\int_{T_a}^{T_b}\int_{\Gamma_s}\left|\nu\frac{\partial u}{\partial y}-\tau_1\right|^2 d\Gamma dt+\frac{\alpha_2}{2}\int_{T_a}^{T_b}\int_{\Gamma_s}\left|-p+2\nu\frac{\partial v}{\partial y}-\tau_2\right|^2 d\Gamma dt\\
&+\frac{\beta_1}{2}\int_{T_0}^{T_1}\int_{\Gamma_a}\left(\left|\frac{\partial g_1}{\partial t}\right|^2+|g_1|^2\right)d\Gamma dt+\frac{\beta_2}{2}\int_{T_0}^{T_1}\int_{\Gamma_a}\left(\left|\frac{\partial g_2}{\partial t}\right|^2+|g_2|^2\right)d\Gamma dt\\
&-\int_0^T\int_\Omega \hat{u}\left(\frac{\partial u}{\partial t}+u\frac{\partial u}{\partial x}+v\frac{\partial u}{\partial y}+\frac{\partial p}{\partial x}-\nu\frac{\partial}{\partial x}\left(2\frac{\partial u}{\partial x}\right)-\nu\frac{\partial}{\partial y}\left(\frac{\partial u}{\partial y}+\frac{\partial v}{\partial x}\right)\right)d\Omega dt\\
&-\int_0^T\int_\Omega \hat{v}\left(\frac{\partial v}{\partial t}+u\frac{\partial v}{\partial x}+v\frac{\partial v}{\partial y}+\frac{\partial p}{\partial y}-\nu\frac{\partial}{\partial x}\left(\frac{\partial u}{\partial y}+\frac{\partial v}{\partial x}\right)-\nu\frac{\partial}{\partial y}\left(2\frac{\partial v}{\partial y}\right)\right)d\Omega dt\\
&-\int_0^T\int_\Omega \hat{p}\left(\frac{\partial u}{\partial x}+\frac{\partial v}{\partial y}\right)d\Omega dt\\
&-\int_{T_0}^{T_1}\int_{\Gamma_a} s_1(u-g_1)d\Gamma dt-\int_0^{T_0}\int_{\Gamma_a} s_1 u\,d\Gamma dt-\int_{T_1}^{T}\int_{\Gamma_a} s_1 u\,d\Gamma dt\\
&-\int_{T_0}^{T_1}\int_{\Gamma_a} s_2(v-g_2)d\Gamma dt-\int_0^{T_0}\int_{\Gamma_a} s_2 v\,d\Gamma dt-\int_{T_1}^{T}\int_{\Gamma_a} s_2 v\,d\Gamma dt
\end{aligned}
\tag{12}
$$

is introduced. In (12), $\hat{u}$ and $\hat{v}$ are Lagrange multipliers that are used to enforce the x and y-components of the momentum equation (1) and (2), respectively, $\hat{p}$ is a Lagrange multiplier that is used to enforce the continuity equation (3), and s_1 and s_2 are Lagrange multipliers that are used to enforce the x and y-components of the boundary condition (5), respectively. Note that Lagrange multipliers have not been introduced to enforce the constraints (4), (6)-(8), and (10), so that these conditions must be required of all candidate functions u, v, p, g_1, and g_2.

Through the introduction of Lagrange multipliers, the constrained optimization problem is converted into the unconstrained problem:

> *find* u, v, p, g_1, g_2, $\hat{u}$, $\hat{v}$, $\hat{p}$, s_1, *and* s_2 *satisfying* (4), (6)-(8), *and* (10)
> *such that the Lagrangian functional* $\mathcal{L}(u,v,p,g_1,g_2,\hat{u},\hat{v},\hat{p},s_1,s_2)$
> *given by* (12) *is rendered stationary.*

In this problem, each argument of the Lagrangian functional is considered to be an independent variable (only subject to the constraints (4), (6)-(8), and (10)) so that each may be varied independently.

The first-order necessary condition that stationary points must satisfy is that the first variation of the Lagrangian with respect to each of its arguments vanishes at those points.

One easily sees that the vanishing of the first variations with respect to the Lagrange multipliers recovers the constraint equations (1)-(3) and (5). Specifically,

$$\begin{aligned}
\frac{\delta\mathcal{L}}{\delta\hat{u}} = 0 \quad &\Longrightarrow \quad x\text{-momentum equation (1)} \\
\frac{\delta\mathcal{L}}{\delta\hat{v}} = 0 \quad &\Longrightarrow \quad y\text{-momentum equation (2)} \\
\frac{\delta\mathcal{L}}{\delta\hat{p}} = 0 \quad &\Longrightarrow \quad \text{continuity equation (3)} \\
\frac{\delta\mathcal{L}}{\delta s_1} = 0 \quad &\Longrightarrow \quad x\text{-component of the boundary condition (5)} \\
\frac{\delta\mathcal{L}}{\delta s_2} = 0 \quad &\Longrightarrow \quad y\text{-component of the boundary condition (5)}\,,
\end{aligned}$$

where $\delta\mathcal{L}/\delta\hat{u}$ denotes the first variation of $\mathcal{L}$ with respect to $\hat{u}$, etc.

3.2. The Adjoint Equations

Next, set the first variations of the Lagrangian with respect to the state variables u, v, and p equal to zero. These result in the *adjoint* or *co-state equations*. Note that, since for the channel flow, candidate solutions must satisfy (4), (6)-(8), and (10), one has that

$$\begin{aligned}
\delta u|_{t=0} = \delta v|_{t=0} = 0 \quad &\text{on } \Omega\,, \\
\delta u|_{\Gamma_i} = \delta v|_{\Gamma_i} = 0 \quad &\text{for } (0,T)\,, \\
\delta u|_{\Gamma_w} = \delta v|_{\Gamma_w} = 0 \quad &\text{for } (0,T)\,, \\
\delta p, \quad \delta u, \quad \delta v, \quad \frac{\partial \delta u}{\partial x}, \quad &\text{and} \quad \frac{\partial \delta v}{\partial x} \to 0 \quad \text{as } x \to \infty \text{ for } (0,T)\,, \text{ and} \\
\delta g_1|_{t=T_0} = \delta g_2|_{t=T_0} = 0 \quad &\text{on } \Gamma_a\,.
\end{aligned} \tag{13}$$

First, consider $\delta\mathcal{L}/\delta p = 0$ which yields

$$\alpha_2 \int_{T_a}^{T_b} \int_{\Gamma_s} \delta p \left(-p + 2\nu \frac{\partial v}{\partial y} - \tau_2 \right) d\Gamma + \int_0^T \int_\Omega \left(\hat{u} \frac{\partial \delta p}{\partial x} + \hat{v} \frac{\partial \delta p}{\partial y} \right) d\Omega dt = 0$$

for arbitrary variations δp in the pressure. Applying Gauss' theorem then yields that

$$\begin{aligned}
\alpha_2 \int_{T_a}^{T_b} \int_{\Gamma_s} \delta p \left(-p + 2\nu \frac{\partial v}{\partial y} - \tau_2 \right) d\Gamma \\
- \int_0^T \int_\Omega \delta p \left(\frac{\partial \hat{u}}{\partial x} + \frac{\partial \hat{v}}{\partial y} \right) d\Omega dt + \int_0^T \int_\Gamma \delta p (\hat{u} n_1 + \hat{v} n_2)\, d\Gamma dt = 0
\end{aligned}$$

where n_1 and n_2 denote the x and y components, respectively, of the outward normal to Ω along Γ. Choosing variations δp that vanish on the boundary Γ but which are arbitrary in the interior Ω of the flow domain yields that

$$\frac{\partial \hat{u}}{\partial x} + \frac{\partial \hat{v}}{\partial y} = 0 \quad \text{on} \quad (0,T) \times \Omega. \tag{14}$$

Now choosing variations δp that are arbitrary along the boundary Γ yields that

$$\hat{u}n_1 + \hat{v}n_2 = \begin{cases} 0 \quad \text{on} \begin{cases} (0,T) \times \Gamma \backslash \Gamma_s \\ (0,T_a) \times \Gamma_s \\ (T_b,T) \times \Gamma_s \end{cases} \\ -\alpha_2 \left(-p + 2\nu \dfrac{\partial v}{\partial y} - \tau_2 \right) \quad \text{on } (T_a,T_b) \times \Gamma_s \,, \end{cases} \tag{15}$$

where $\Gamma \backslash \Gamma_s$ denotes the boundary Γ with Γ_s deleted. We note that in the above derivation of (14) and (15), as in the derivations found below, the boundary integrals at infinity do not make any contribution due to the fourth equation of (13).

Next, consider $\delta \mathcal{L}/\delta v = 0$ which yields

$$\begin{aligned} -\alpha_2 \int_{T_a}^{T_b} \int_{\Gamma_s} & 2\nu \frac{\partial \delta v}{\partial y} \left(-p + 2\nu \frac{\partial v}{\partial y} - \tau_2 \right) d\Gamma \\ & + \int_0^T \int_\Omega \left(\hat{u}\delta v \frac{\partial u}{\partial y} - \nu \hat{u} \frac{\partial^2 \delta v}{\partial x \partial y} + \hat{p} \frac{\partial \delta v}{\partial y} \right) d\Omega dt \\ & + \int_0^T \int_\Omega \hat{v} \left(\frac{\partial \delta v}{\partial t} + u \frac{\partial \delta v}{\partial x} + \delta v \frac{\partial v}{\partial y} + v \frac{\partial \delta v}{\partial y} - \nu \frac{\partial^2 \delta v}{\partial x^2} - 2\nu \frac{\partial^2 \delta v}{\partial y^2} \right) d\Omega dt \\ & + \int_{T_0}^{T_1} \int_{\Gamma_a} s_2 \delta v d\Gamma dt + \int_0^{T_0} \int_{\Gamma_a} s_2 \delta v d\Gamma dt + \int_{T_1}^{T} \int_{\Gamma_a} s_2 \delta v d\Gamma dt = 0 \,. \end{aligned}$$

Applying Gauss' theorem enough times to remove all derivatives from the variation δv in

the integrals on Ω yields

$$
\begin{aligned}
-\alpha_2 \int_{T_a}^{T_b} \int_{\Gamma_s} 2\nu \frac{\partial \delta v}{\partial y} \left(-p + 2\nu \frac{\partial v}{\partial y} - \tau_2 \right) d\Gamma \\
+ \int_0^T \int_\Omega \delta v \Bigg(-\frac{\partial \hat{v}}{\partial t} - \hat{v} \frac{\partial u}{\partial x} - \hat{v} \frac{\partial v}{\partial y} + \hat{u} \frac{\partial u}{\partial y} + \hat{v} \frac{\partial v}{\partial y} \\
- u \frac{\partial \hat{v}}{\partial x} - v \frac{\partial \hat{v}}{\partial y} - \frac{\partial \hat{p}}{\partial y} - \nu \frac{\partial^2 \hat{u}}{\partial x \partial y} - \nu \frac{\partial^2 \hat{v}}{\partial x^2} - 2\nu \frac{\partial^2 \hat{v}}{\partial y^2} \Bigg) d\Omega dt \\
+ \int_\Omega (\hat{v} \delta v)|_{t=T} d\Omega \\
+ \int_0^T \int_{\Gamma_a} \delta v \left(s_2 + \hat{p} n_2 + \hat{v} u n_1 + \hat{v} v n_2 + \nu \frac{\partial \hat{u}}{\partial y} n_1 + \nu \frac{\partial \hat{v}}{\partial x} n_1 + 2\nu \frac{\partial \hat{v}}{\partial y} n_2 \right) d\Gamma dt \\
-\nu \int_0^T \int_\Gamma \left(\hat{v} \frac{\partial \delta v}{\partial x} n_1 + 2\hat{v} \frac{\partial \delta v}{\partial y} n_2 + \hat{u} \frac{\partial \delta v}{\partial x} n_2 \right) d\Gamma dt = 0 \,,
\end{aligned}
\tag{16}
$$

where we have used (13) to eliminate boundary integrals along Γ_i, Γ_w and as $x \to \infty$ and an integral over Ω at $t = 0$. First, variations δv that vanish at $t = 0$, $t = T$, and in a neighborhood of Γ are chosen, but which are otherwise arbitrary. Such a choice implies that all boundary integrals in (16) vanish giving

$$
\begin{aligned}
-\frac{\partial \hat{v}}{\partial t} + \hat{u} \frac{\partial u}{\partial y} + \hat{v} \frac{\partial v}{\partial y} - u \frac{\partial \hat{v}}{\partial x} - v \frac{\partial \hat{v}}{\partial y} - \frac{\partial \hat{p}}{\partial y} \\
-\nu \frac{\partial}{\partial x} \left(\frac{\partial \hat{u}}{\partial y} + \frac{\partial \hat{v}}{\partial x} \right) - \nu \frac{\partial}{\partial y} \left(2 \frac{\partial \hat{v}}{\partial y} \right) = 0 \quad \text{in} \quad (0,T) \times \Omega \,,
\end{aligned}
\tag{17}
$$

where equation (3) is used to effect a simplification. Next, variations that vanish in a neighborhood of Γ, but which are otherwise arbitrary, are chosen to obtain

$$
\hat{v}|_{t=T} = 0 \quad \text{in} \quad \Omega \,. \tag{18}
$$

Now, along Γ, δv and $\partial \delta v / \partial n$ may be independently selected, provided that (13) is satisfied, where $\partial / \partial n$ denotes the derivative in the direction of the outward normal to Ω along Γ. If $\delta v = 0$ and $\partial \delta v / \partial n$ varies arbitrarily along Γ, then

$$
\hat{v} = \begin{cases}
0 \quad \text{on} \begin{cases} (0,T) \times \Gamma \backslash \Gamma_s \\ (0,T_a) \times \Gamma_s \\ (T_b,T) \times \Gamma_s \end{cases} \\
\alpha_2 \left(-p + 2\nu \dfrac{\partial v}{\partial y} - \tau_2 \right) \quad \text{on } (T_a,T_b) \times \Gamma_s \,.
\end{cases}
\tag{19}
$$

To see this, note that along the inflow, Γ_i, $n_2 = 0$ and $\partial/\partial n = -\partial/\partial x$ while along the top and bottom boundaries $n_1 = 0$, $\partial/\partial n = \pm\partial/\partial y$, respectively, and, since $\delta v = 0$, $\partial \delta v/\partial x = 0$. Note that (15) and (19) agree on the boundary segments where they simultaneously apply. Finally, δv is arbitrarily chosen along Γ_a to obtain

$$s_2 = -\hat{p}n_2 - \hat{v}(un_1 + vn_2) - \nu\left(\frac{\partial \hat{u}}{\partial y} + \frac{\partial \hat{v}}{\partial x}\right)n_1 - 2\nu\frac{\partial \hat{v}}{\partial y}n_2 \quad \text{on} \quad (0,T)\times\Gamma_a\,. \tag{20}$$

Next, consider $\delta\mathcal{L}/\delta u = 0$ which yields

$$\begin{aligned}
-\alpha_1 \int_{T_a}^{T_b}\int_{\Gamma_s} \nu\frac{\partial \delta u}{\partial y}\left(\nu\frac{\partial u}{\partial y} - \tau_1\right) d\Gamma \\
+\int_0^T\int_\Omega \hat{u}\left(\frac{\partial \delta u}{\partial t} + u\frac{\partial \delta u}{\partial x} + \delta u\frac{\partial u}{\partial x} + v\frac{\partial \delta u}{\partial y} - 2\nu\frac{\partial^2 \delta u}{\partial x^2} - \nu\frac{\partial^2 \delta u}{\partial y^2}\right) d\Omega dt \\
+\int_0^T\int_\Omega \left(\hat{v}\delta u\frac{\partial v}{\partial x} - \nu\hat{v}\frac{\partial^2 \delta u}{\partial x \partial y} + \hat{p}\frac{\partial \delta u}{\partial x}\right) d\Omega dt + \int_0^T\int_{\Gamma_a} s_1\delta u\, d\Gamma dt = 0\,.
\end{aligned}$$

Applying Gauss' theorem enough times to remove all derivatives from the variation δu in the integrals on Ω yields

$$\begin{aligned}
-\alpha_1 \int_{T_a}^{T_b}\int_{\Gamma_s} \nu\frac{\partial \delta u}{\partial y}\left(\nu\frac{\partial u}{\partial y} - \tau_1\right) d\Gamma \\
+\int_0^T\int_\Omega \delta u\Big(-\frac{\partial \hat{u}}{\partial t} - \hat{u}\frac{\partial u}{\partial x} - \hat{u}\frac{\partial v}{\partial y} + \hat{u}\frac{\partial u}{\partial x} + \hat{v}\frac{\partial v}{\partial x} \\
-u\frac{\partial \hat{u}}{\partial x} - v\frac{\partial \hat{u}}{\partial y} - \frac{\partial \hat{p}}{\partial x} - 2\nu\frac{\partial^2 \hat{u}}{\partial x^2} - \nu\frac{\partial^2 \hat{u}}{\partial y^2} - \nu\frac{\partial^2 \hat{v}}{\partial x \partial y}\Big) d\Omega dt \\
+\int_\Omega (\hat{u}\delta u)|_{t=T} d\Omega \\
+\int_0^T\int_{\Gamma_a} \delta u\left(s_1 + \hat{p}n_1 + \hat{u}un_1 + \hat{u}vn_2 + 2\nu\frac{\partial \hat{u}}{\partial x}n_1 + \nu\frac{\partial \hat{u}}{\partial y}n_2 + \nu\frac{\partial \hat{v}}{\partial x}n_2\right) d\Gamma dt \\
-\nu\int_0^T\int_\Gamma \left(2\hat{u}\frac{\partial \delta u}{\partial x}n_1 + \hat{u}\frac{\partial \delta u}{\partial y}n_2 + \hat{v}\frac{\partial \delta u}{\partial y}n_1\right) d\Gamma dt = 0\,.
\end{aligned}$$

Applying to this equation the same process that led from (16) to (17)-(20) yields

$$\begin{aligned}
-\frac{\partial \hat{u}}{\partial t} + \hat{u}\frac{\partial u}{\partial x} + \hat{v}\frac{\partial v}{\partial x} - u\frac{\partial \hat{u}}{\partial x} - v\frac{\partial \hat{u}}{\partial y} - \frac{\partial \hat{p}}{\partial x} \\
-\nu\frac{\partial}{\partial x}\left(2\frac{\partial \hat{u}}{\partial x}\right) - \nu\frac{\partial}{\partial y}\left(\frac{\partial \hat{u}}{\partial y} + \frac{\partial \hat{v}}{\partial x}\right) = 0 \quad \text{in} \quad (0,T)\times\Omega\,.
\end{aligned} \tag{21}$$

$$\hat{u}\big|_{t=T} = 0 \quad \text{in} \quad \Omega, \tag{22}$$

$$\hat{u} = \begin{cases} 0 \quad \text{on} \begin{cases} (0,T)\times\Gamma\backslash\Gamma_s \\ (0,T_a)\times\Gamma_s \\ (T_b,T)\times\Gamma_s \end{cases} \\ \alpha_1\left(\nu\dfrac{\partial u}{\partial y} - \tau_1\right) \quad \text{on } (T_a,T_b)\times\Gamma_s\,, \end{cases} \tag{23}$$

and

$$s_1 = -\hat{p}n_1 - \hat{u}(un_1+vn_2) - 2\nu\frac{\partial\hat{u}}{\partial x}n_1 - \nu\left(\frac{\partial\hat{u}}{\partial y}+\frac{\partial\hat{v}}{\partial x}\right)n_2 \quad \text{on} \quad (0,T)\times\Gamma_a\,. \tag{24}$$

In deriving (23) we have used the assumption that Γ_s is part of the lower boundary of the channel so that along Γ_s we have that $n_2 = -1$. Again, there is no conflict between (15) and (23) along boundary segments on which both apply.

3.3. The Optimality Conditions

The only first-order necessary conditions left to consider are $\delta\mathcal{L}/\delta g_1 = 0$ and $\delta\mathcal{L}/\delta g_2 = 0$. (These conditions are usually called the *optimality conditions*.) Now, since all candidate functions g_1 and g_2 must statisfy (10), it follows that $\delta g_1 = 0$ and $\delta g_2 = 0$ at $t = T_0$. Then, $\delta\mathcal{L}/\delta g_2 = 0$ yields that

$$\beta_2\int_{T_0}^{T_1}\int_{\Gamma_a}\left(\frac{\partial g_2}{\partial t}\frac{\partial\delta g_2}{\partial t} + g_2\delta g_2\right)d\Gamma dt + \int_{T_0}^{T_1}\int_{\Gamma_a} s_2\delta g_2\, d\Gamma dt = 0\,.$$

Applying Gauss' theorem to remove all derivatives from the variation δg_2 yields

$$\int_{T_0}^{T_1}\int_{\Gamma_a}\delta g_2\left(-\frac{\partial^2 g_2}{\partial t^2} + g_2 + \frac{1}{\beta_2}s_2\right)d\Gamma dt + \int_{\Gamma_a}\left(\delta g_2\frac{\partial g_2}{\partial t}\right)\Big|_{t=T_1} d\Gamma = 0\,,$$

where the fact that $\delta g_2\big|_{t=T_0} = 0$ has been used. Choosing variations δg_2 that vanish at $t = T_1$ but which are otherwise arbitrary yields

$$-\frac{\partial^2 g_2}{\partial t^2} + g_2 = -\frac{1}{\beta_2}s_2 \quad \text{on} \quad (T_0\,,T_1)\times\Gamma_a$$

or, using (20),

$$-\frac{\partial^2 g_2}{\partial t^2} + g_2 = -\frac{1}{\beta_2}\left(\hat{p} + 2\nu\frac{\partial\hat{v}}{\partial y}\right) \quad \text{on} \quad (T_0\,,T_1)\times\Gamma_a\,, \tag{25}$$

where (19) and the assumption that Γ_a is part of the lower boundary so that, along Γ_a, $n_1 = 0$ and $n_2 = -1$ have been used. Now, choosing variations that are arbitrary at $t = T_1$ yields that $\partial g_2/\partial t = 0$ along Γ_a at $t = T_1$ so that, invoking (10), $g_2(t,x)$ satisfies

$$g_2|_{t=T_0} = g_{20}(x) \qquad \text{and} \qquad \left.\frac{\partial g_2}{\partial t}\right|_{t=T_1} = 0 \qquad \text{on } \Gamma_a\,. \tag{26}$$

Note that, given $\hat{p}$ and $\hat{v}$, (25)-(26) constitute, at each point $x \in \Gamma_a$, a two-point boundary value problem in time over the interval (T_0, T_1).

In a similar manner, setting $\delta\mathcal{L}/\delta g_1 = 0$ yields that

$$-\frac{\partial^2 g_1}{\partial t^2} + g_1 = -\frac{1}{\beta_1}\left(\nu\frac{\partial \hat{u}}{\partial y}\right) \quad \text{on } (T_0, T_1) \times \Gamma_a \tag{27}$$

and

$$g_1|_{t=T_0} = g_{10}(x) \qquad \text{and} \qquad \left.\frac{\partial g_1}{\partial t}\right|_{t=T_1} = 0 \qquad \text{on } \Gamma_a\,. \tag{28}$$

3.4. Finite Computational Domains

In the computations, the semi-infinte domain Ω (we are still only considering the channel flow case) is replaced by a finite domain Ω_C defined by the introduction of the outflow boundary Γ_o given by $[x = L,\, 0 \le y \le h]$. Thus, we have that Ω_C is the rectangle $[0 \le x \le L,\, 0 \le y \le h]$. We treat the ouflow by replacing (1) and (2) with

$$\frac{\partial u}{\partial t} + u\frac{\partial u}{\partial x} + v\frac{\partial u}{\partial y} + \frac{\partial p}{\partial x} - \nu a(x)\frac{\partial^2 u}{\partial x^2} - \nu\frac{\partial^2 u}{\partial y^2} = 0 \quad \text{in } (0,T) \times \Omega_C, \tag{29}$$

and

$$\frac{\partial v}{\partial t} + u\frac{\partial v}{\partial x} + v\frac{\partial v}{\partial y} + \frac{\partial p}{\partial y} - \nu a(x)\frac{\partial^2 v}{\partial x^2} - \nu\frac{\partial^2 v}{\partial y^2} = 0 \quad \text{in } (0,T) \times \Omega_C, \tag{30}$$

respectively, where $a(x)$ is a smooth function that is unity in the bulk of the flow, that vanishes in a neighborhood of the outflow boundary Γ_o, and which is smooth throughout the flow. This treatment of the outflow does not require the imposition of boundary conditions along the outflow boundary Γ_o (Streett & Macaraeg, 1989) zone technique.

A similar treatment of the adjoint variables should have required consideration of an infinite domain $[-\infty < x < \infty,\, 0 < y < h]$. If this had been done, the boundary conditions (19) and (23) would not have been obtained along the inflow Γ_i. In fact, the inflow boundary Γ_i for the state equation is the outflow boundary for the adjoint equations and, conversely, the outflow boundary Γ_o for the state equation is the inflow boundary for

the adjoint equations. This is easily seen by comparing the leading inertial terms of the state and adjoint momentum equations (1), (2), (21), and (17), i.e., with t increasing

$$\frac{\partial u}{\partial t} + u\frac{\partial u}{\partial x} + v\frac{\partial u}{\partial y} \quad \text{and} \quad \frac{\partial v}{\partial t} + u\frac{\partial v}{\partial x} + v\frac{\partial v}{\partial y}$$

and with t decreasing

$$-\frac{\partial \hat{u}}{\partial t} - u\frac{\partial \hat{u}}{\partial x} - v\frac{\partial \hat{u}}{\partial y} \quad \text{and} \quad -\frac{\partial \hat{v}}{\partial t} - u\frac{\partial \hat{v}}{\partial x} - v\frac{\partial \hat{v}}{\partial y}\,.$$

Now, on both Γ_i and Γ_o we have that $u > 0$ and $v \approx 0$ which is why Γ_i is an inflow boundary and Γ_o is an outflow boundary for the state. On the other hand, the fact that t is decreasing in the adjoint equations implies that now Γ_i is an outflow boundary and Γ_o is an inflow boundary for those equations.

Thus, to be consistent with the treatment of the state equations, the adjoint outflow Γ_i should be treated in a manner similar to the above treatment of the state outflow Γ_o. Thus, the boundary conditions (19) and (23) are not imposed along Γ_i and (21) and (17) are replaced by

$$\begin{aligned} -\frac{\partial \hat{u}}{\partial t} + \hat{u}\frac{\partial u}{\partial x} + \hat{v}\frac{\partial v}{\partial x} - u\frac{\partial \hat{u}}{\partial x} - v\frac{\partial \hat{u}}{\partial y} - \frac{\partial \hat{p}}{\partial x} \\ -\nu b(x)\frac{\partial^2 \hat{u}}{\partial x^2} - \nu\frac{\partial^2 \hat{u}}{\partial y^2} = 0 \quad \text{in} \quad (0,T)\times\Omega_C \end{aligned} \tag{31}$$

and

$$\begin{aligned} -\frac{\partial \hat{v}}{\partial t} + \hat{u}\frac{\partial u}{\partial y} + \hat{v}\frac{\partial v}{\partial y} - u\frac{\partial \hat{v}}{\partial x} - v\frac{\partial \hat{v}}{\partial y} - \frac{\partial \hat{p}}{\partial y} \\ -\nu b(x)\frac{\partial^2 \hat{v}}{\partial x^2} - \nu\frac{\partial^2 \hat{v}}{\partial y^2} = 0 \quad \text{in} \quad (0,T)\times\Omega_C\,, \end{aligned} \tag{32}$$

respectively, where $b(x)$ is a smooth function that is unity in the bulk of the flow, that vanishes in a neighborhood of the adjoint outflow boundary Γ_i, and which is smooth throughout the flow. This treatment of the adjoint outflow does not require the imposition of any boundary conditions for the adjoint variables along Γ_i. Finally, since Γ_o is an inflow boundary for the adjoint equations, one should specify boundary conditions on the adjoint variables along that boundary segment. It can be seen that the proper conditions are given by

$$\hat{u} = 0 \quad \text{and} \quad \hat{v} = 0 \quad \text{on} \quad (0,T)\times\Gamma_o\,. \tag{33}$$

3.5. The Optimality System for Channel Flow

We now have in hand the full *optimality system* for channel flow whose solutions determine the optimal states, controls, and adjoint states. These are given by (3)-(7), (14), (15), (18)-(20), and (22)-(33), where in (19) and (23) we do not impose the boundary conditions along Γ_i. Since (20) and (24) merely serve to determine the uninteresting Lagrange multipliers s_2 s_1, respectively, they can be ignored. Re-ordering and gathering the remaining equations, posed on the computational domain Ω_C, yields the optimality system

$$\frac{\partial u}{\partial t} + u\frac{\partial u}{\partial x} + v\frac{\partial u}{\partial y} + \frac{\partial p}{\partial x} - \nu a(x)\frac{\partial^2 u}{\partial x^2} - \nu\frac{\partial^2 u}{\partial y^2} = 0 \quad \text{in } (0,T)\times\Omega_C\,, \tag{34}$$

$$\frac{\partial v}{\partial t} + u\frac{\partial v}{\partial x} + v\frac{\partial v}{\partial y} + \frac{\partial p}{\partial y} - \nu a(x)\frac{\partial^2 v}{\partial x^2} - \nu\frac{\partial^2 v}{\partial y^2} = 0 \quad \text{in } (0,T)\times\Omega_C\,, \tag{35}$$

$$\frac{\partial u}{\partial x} + \frac{\partial v}{\partial y} = 0 \quad \text{in } (0,T)\times\Omega_C\,, \tag{36}$$

$$\begin{pmatrix} u \\ v \end{pmatrix}\Big|_{t=0} = \begin{pmatrix} u_0 \\ v_0 \end{pmatrix} \quad \text{in } \Omega_C\,, \tag{37}$$

$$\begin{pmatrix} u \\ v \end{pmatrix}\Big|_{\Gamma_a} = \begin{cases} \begin{pmatrix} g_1 \\ g_2 \end{pmatrix} & \text{in } (T_0\,,T_1) \\ \begin{pmatrix} 0 \\ 0 \end{pmatrix} & \text{in } (0,T_0) \text{ and } (T_1,T)\,, \end{cases} \tag{38}$$

$$\begin{pmatrix} u \\ v \end{pmatrix}\Big|_{\Gamma_i} = \begin{pmatrix} u_i \\ v_i \end{pmatrix} \quad \text{in } \ (0,T)\,, \tag{39}$$

$$\begin{pmatrix} u \\ v \end{pmatrix}\Big|_{\Gamma_w} = \begin{pmatrix} 0 \\ 0 \end{pmatrix} \quad \text{in } \ (0,T)\,, \tag{40}$$

$$-\frac{\partial \hat{u}}{\partial t} + \hat{u}\frac{\partial u}{\partial x} + \hat{v}\frac{\partial v}{\partial x} - u\frac{\partial \hat{u}}{\partial x} - v\frac{\partial \hat{u}}{\partial y} - \frac{\partial \hat{p}}{\partial x} - \nu b(x)\frac{\partial^2 \hat{u}}{\partial x^2} - \nu\frac{\partial^2 \hat{u}}{\partial y^2} = 0 \quad \text{in } \ (0,T)\times\Omega_C\,, \tag{41}$$

$$-\frac{\partial \hat{v}}{\partial t} + \hat{u}\frac{\partial u}{\partial y} + \hat{v}\frac{\partial v}{\partial y} - u\frac{\partial \hat{v}}{\partial x} - v\frac{\partial \hat{v}}{\partial y} - \frac{\partial \hat{p}}{\partial y} - \nu b(x)\frac{\partial^2 \hat{v}}{\partial x^2} - \nu\frac{\partial^2 \hat{v}}{\partial y^2} = 0 \quad \text{in } \ (0,T)\times\Omega_C\,, \tag{42}$$

$$\frac{\partial \hat{u}}{\partial x} + \frac{\partial \hat{v}}{\partial y} = 0 \quad \text{in } \ (0,T)\times\Omega_C\,, \tag{43}$$

$$\begin{pmatrix} \hat{u} \\ \hat{v} \end{pmatrix}\Big|_{t=T} = \begin{pmatrix} 0 \\ 0 \end{pmatrix} \quad \text{in } \ \Omega_C\,, \tag{44}$$

$$\begin{pmatrix} \hat{u} \\ \hat{v} \end{pmatrix} = \begin{pmatrix} 0 \\ 0 \end{pmatrix} \quad \text{on} \quad \begin{cases} (0,T) \times \Gamma_o \\ (0,T) \times \Gamma_a \\ (0,T) \times \Gamma_w \backslash \Gamma_s \\ (0,T_a) \times \Gamma_s \\ (T_b,T) \times \Gamma_s \, , \end{cases} \tag{45}$$

$$\begin{pmatrix} \hat{u} \\ \hat{v} \end{pmatrix} = - \begin{pmatrix} \alpha_1 \left(\nu \frac{\partial u}{\partial y} - \tau_1 \right) \\ \alpha_2 \left(-p + 2\nu \frac{\partial v}{\partial y} - \tau_2 \right) \end{pmatrix} \quad \text{on} \quad (T_a, T_b) \times \Gamma_s \, , \tag{46}$$

$$-\frac{\partial^2 g_1}{\partial t^2} + g_1 = -\frac{1}{\beta_1} \left(\nu \frac{\partial \hat{u}}{\partial y} \right) \quad \text{on} \quad (T_0, T_1) \times \Gamma_a \, , \tag{47}$$

$$g_1|_{t=T_0} = g_{10}(x) \qquad \text{and} \qquad \left. \frac{\partial g_1}{\partial t} \right|_{t=T_1} = 0 \qquad \text{on} \quad \Gamma_a \, , \tag{48}$$

$$-\frac{\partial^2 g_2}{\partial t^2} + g_2 = -\frac{1}{\beta_2} \left(\hat{p} + 2\nu \frac{\partial \hat{v}}{\partial y} \right) \quad \text{on} \quad (T_0, T_1) \times \Gamma_a \, , \tag{49}$$

and

$$g_2|_{t=T_0} = g_{20}(x) \qquad \text{and} \qquad \left. \frac{\partial g_2}{\partial t} \right|_{t=T_1} = 0 \qquad \text{on} \quad \Gamma_a \, , \tag{50}$$

where Γ_w denotes, in the channel flow case, the upper and lower boundaries of the *finite* channel except for the segment Γ_a.

The state equations (34)-(40) are driven by the given initial velocity (u_0, v_0), the given inflow velocity (u_i, v_i), and the controls (g_1, g_2). Indeed, the purpose of this study is to determine g_1 and g_2 that optimally counteracts instabilities created upstream of Γ_a. The adjoint equations (41)-(46) are homogeneous execept for the boundary condition (46) along Γ_s, the part of the boundary along which we are trying to match the stresses. The data in that boundary condition is exactly the discrepancy between the desired stresses τ_1 and τ_2 and the stresses $\nu \partial u/\partial y$ and $-p + 2\nu \partial u/\partial y$ along Γ_s, weighted by the factors α_1 and α_2. The equations for the controls (47)-(50) are driven by the negative of the adjoint stresses along Γ_a, the part of the boundary along which we apply the control, weighted by the factors $1/\beta_1$ and $1/\beta_2$. Of course this division into equations for the state, the adjoint state, and the control is really obscured by the fact that (34)-(50) are all intimitately coupled.

3.6. The Optimality System for Boundary-Layer Flow

Following a similar process to that used in Sections 3.1-3.5 for the channel flow case, one may derive an optimality system for the boundary layer flow case. The only difference is that in the latter case Γ_w denotes only the lower boundary with Γ_a excluded and that the additional boundary condition (9) along the upper boundary Γ_e must be accounted for.

With the new interpretation for Γ_w, one can still define the Lagrangian functional (12) and use the constraints (13) on allowable variations; however, due to (9), allowable variations are further constrained by

$$\delta u|_{\Gamma_e} = \left(\delta p - 2\nu \frac{\partial \delta v}{\partial y}\right)\Big|_{\Gamma_e} = 0 \quad \text{for } (0,T)\,. \tag{51}$$

Note that (51) implies that, along Γ_e, one may not choose the variations in δp and $\partial \delta v/\partial y$ independently. Considering, simultaneously, variations in p, v, and $\partial v/\partial y$ along Γ_e, one obtains

$$\begin{aligned} &\int_0^T \int_{\Gamma_e} \hat{v}\left(\delta p - 2\nu \frac{\partial \delta v}{\partial y}\right) d\Gamma dt \\ &\qquad + \int_0^T \int_{\Gamma_e} \delta v \left(\hat{p} + 2\nu \frac{\partial \hat{v}}{\partial y} + \hat{v} v\right) d\Gamma dt - \int_0^T \int_{\Gamma_e} \hat{u} \frac{\partial \delta v}{\partial x}\, d\Gamma dt = 0\,. \end{aligned} \tag{52}$$

The first integral in (52) vanishes due to (51). One can show that

$$\hat{u} = 0 \quad \text{on } (0,T) \times \Gamma_e \tag{53}$$

so that the third integral in (52) vanishes as well. Then, letting δv be arbitrary along Γ_e in (52) yields

$$\hat{p} + 2\nu \frac{\partial \hat{v}}{\partial y} + v\hat{v} = 0 \quad \text{on } (0,T) \times \Gamma_e\,. \tag{54}$$

The resulting optimality system for the boundary layer flow case is given by (9), (34)-(50), (53), and (54), where in (40) and (45) Γ_w notes the *finite* computational lower boundary with Γ_a excluded and in (53) and (54) Γ_e denotes the *finite* computational uppper boundary.

4. NUMERICAL EXPERIMENTS

Here, the optimal control methodology developed in Section 3 is applied to a boundary layer flow having a single instability wave that can be characterized by a discrete frequency within the spectrum. We are not concerned with the details of how disturbances are ingested into the boundary layer; the underlying assumption here is that natural transition involves some dominant disturbances that can be characterized by waves, and in fact, in the present study, by a single wave. (In a subsequent study, controlling transitions which consist of unsteady, three-dimensional instabilities will be explored.) As described in Joslin et al. (1995) (among others), these discrete small-amplitude instabilities can be suppressed through *wave cancellation* (WC) using known exact information concerning the wave. Hence, the optimal control is "known" for validation of the present DNS/optimal control theory numerical approach in which the instability is to be suppressed without any a priori knowledge of said instability.

The formidable coupled system (9), (34)-(50), (53), and (54) is solved in an iterative manner. First, a guess is made for the controls g_1 and g_2 (typically one starts with no control, i.e., $g_1 = g_2 = 0$) and then the sub-system (9) and (34)-(40) is solved for the state variables, i.e., the velocity field (u, v) and pressure p. Then, using these velocity and pressure fields, the sub-system (41)-(46), (53), and (54) is solved for the adjoint or co-state variables $(\hat{u}, \hat{v})$ and $\hat{p}$. Then, using these adjoint variables, the controls g_1 and g_2 are then found by solving the sub-system (47)-(50). The procedure is repeated until satisfactory convergence is achieved.

The nonlinear, unsteady Navier-Stokes equations and linear adjoint Navier-Stokes equations are solved by direct numerical simulation (DNS) of disturbances that evolve spatially within the boundary layer. The spatial DNS approach involves spectral and high-order finite-difference methods (Joslin *et al* 1992, 1993) and a three-stage Runge-Kutta method (Williamson 1980) for time advancement. The influence-matrix technique is employed to solve the resulting pressure equation (Danabasoglu, Biringen & Streett 1991 and Street & Hussaini 1991). Disturbances are forced into the boundary layer by unsteady suction and blowing through a slot in the wall. At the outflow boundary, the buffer-domain technique of Streett & Macaraeg (1989) is used.

In the present study only normal injection or suction control is allowed, so that we set $g_1 = 0$ in (38), $\beta_1 = 0$ in the functional (11), and ignore (47) and (48). Also, we only match the normal stress along Γ_s so that we choose $\alpha_1 = 0$ in the functional (11) and in (46).

4.1. Computational Parameters

For the computations, the grid has 401 streamwise and 41 wall-normal points. The free stream boundary is located $75\delta_o^*$ from the wall, and the streamwise length is $224\delta_o^*$ which is equal to approximately 8 TS wavelengths. The nondimensional frequency for the forced disturbance is $F = \omega/R \times 10^6 = 86$; the forcing amplitude is $v_f = 0.1\%$. The Reynolds number based on the inflow displacement thickness (δ_o^*) is $R = 900$. (The boundary segment along which disturbance forcing and control is effected as well as where stress matching occurs are located within the unstable region of the linear stability neutral curve.) A time-step size corresponding to 320 steps per period T_p is chosen for a three-stage Runge-Kutta method. Based on the disturbance frequency, a characteristic period can be defined as $T_p = 2\pi/\omega = 81.1781$; the resulting time-step size is then $\Delta t = 0.2537$.

To complete one period of the active-control simulation process, 0.75 minutes on the Cray C-90 are required using a single processor. Note, two periods of cost ($T_a \rightarrow T_b$ and $T_b \rightarrow T_a$) are required to complete one iteration of the DNS/adjoint system. Although in general any time interval may be specified for $T_a \rightarrow T_b$, this study uses integer increments of the period (T_p) for simplicity. Hence, $T_a \rightarrow T_b = 2T_p$ would cost $4T_p$ in computations, or roughly 3 min of C-90 time per iteration. Because only a single small-amplitude wave (linear) is forced, the above grid is more than adequate; however, a grid refinement was performed and produced results equivalent to the results reported here.

For this study, the disturbance forcing slot Γ_f, the control or actuator orifice Γ_a, and the matching or sensor segment Γ_s have equal length $4.48\delta_o^*$. The forcing is centered downstream at $389.62\delta_o^*$ (the Reynolds number based on the displacement thickness at that location is $R = 1018.99$), the actuator is centered at $403.62\delta_o^*$ ($R = 1037.13$), and the sensor is centered at $417.62\delta_o^*$ ($R = 1054.97$). These separation distances were arbitrarily chosen for this demonstration. In practice, the control and matching segments should have a minimal separation distance so that the pair can be packaged as a single unit, or bundle, for distributed application of many bundles.

4.2. Results

All simulations allow the flow field to develop for one period, i.e., from $t = 0 \rightarrow T_a = T_p$ before control is initiated. In the first series of simulations, the interval during which control is applied is arbitrarily chosen to be $T_a \rightarrow T_b = 2T_p$. Based on $\alpha_1 = \beta_1 = 0$, $\alpha_2 = 1$, and $\beta_2 = 10$, the wall-normal velocity and disturbance energy results are shown in Figure 2 for the series of iterations leading to convergence. Figure 3 shows the convergence history

for the actuator g_2 and measured normal stress $-p + 2\nu\partial v/\partial y$ as a function of time. The velocities are obtained at a fixed distance from the wall corresponding to $1.18\delta_o^*$ and the measure of energy is given by $E = \int_y u^2 + v^2$; both velocity and energy are obtained at the fixed time T_b. Convergence is obtained with 8 iterations; however, for all practical purposes, the results with 4 iterations could be used. The results demonstrate that a measure of wave cancellation can be obtained from the DNS/control theory system. The wall-normal amplitude of the modified wave at $R = 1092.5$ is 40 percent of the uncontrolled wave; the control without optimizing the choice of α_1, α_2, β_1, and β_2 has led to a 60 percent decrease in the amplitude of the travelling wave. Clearly, Figure 2 shows that a net reduction of the disturbance energy is obtained by energy input due to the control. This results in a delay of transition by-way-of a suppression of the instability evolution.

In the simulation, the control has been applied from $T_a \rightarrow T_b$ only; therefore, for $t > T_b$, (5) or (38) indicate that the actuation is discontinued. Figures 4 and 5 compare the converged results (C1=8th iteration of Figures 2 and 3) with results for one period after control $t = T_b + T_p$. The measured disturbance tends toward the uncontrolled solution when the actuation is discontinued (as expected); because the control was applied for $T_a - T_p \rightarrow T_b = 2T_p$, 2 periods are required after T_b before the computed solution in the window exactly matches the uncontrolled solution. The profiles of uncontrolled, control, and discontinued control flows are shown in Figure 5 at the downstream location corresponding to $R = 1073.2$. Clearly, the control only removes energy from the system (decreases the wave instability amplitude); the resulting profiles retain the expected instability profile shape.

The effect of varying the window size (T_a, T_b) is shown in Figures 6 and 7. The previous converged results (C1) are shown with converged results (C2) for the extended window ($T_a = T_p \rightarrow T_b = 3T_p$). The results are identical for the first two periods of time and indicate that extending the amount of time for control serves to extend control only. This result also indicates that one can solve for the optimal control over a given time interval (T_a, T_b) by breadking up that inerval and solving for the optimal control over a series of smaller subintervals. This approach usually leads to substantial savings in CPU and memory costs.

Figure 7 reveals an additional insight about the present DNS/control theory. The resulting optimal control g_2 approaches the desired wave-cancellation time-periodic solution as the temporal length (T_a, T_b) is increased. This is convincing evidence that the present self-contained methodology is valid.

Figures 8 and 9 show velocity contours of the uncontrolled and controlled (C2) instability waves. Both results indicate that the instability wave is growing with downstream distance (left-to-right); however, the C2 contours are significantly reduced in magnitude. The furthest downstream levels of C2 approach the level of the uncontrolled wave at the furthest upstream location. If the growth rates are assumed to be the same, then a three-wavelength transition delay has been achieved by applying the optimal control.

The instability wave resulting from wave-cancellation (WC) is shown with the control (C2) in Figures 10 and 11. For the present comparison, the amplitude of the actuation for WC was adjusted until nearly exact wave cancellation was achieved. Although the DNS/control theory did not achieve the same level of energy removal, the similar effect of WC was achieved without any a priori knowledge of the instability. Also, note that Figure 11 shows that the optimal control of the control theory has nearly the exact phase characteristics as WC and only lacks the necessary amplitude for additional wave cancellation. These encouraging results suggest that by the appropriate selection of α_1, α_2, β_1, and β_2, the optimal control can be made nearly as effective method of instability suppression as exact wave cancellation.

From the wave-cancellation study of Joslin *et al* (1995), the relationship between amplitude of the actuator (v_a) with resulting instabilty can be shown in Figure 12. A similar result was shown in the channel flow wave-cancellation study in Biringen (1984). The trend indicates, that beginning with a small actuation amplitude, as the actuation level is increased, the amount of wave cancellation (energy extraction from the disturbance) increases. At some optimal actuation, nearly exact wave cancellation is achieved for the instability wave. As the actuation amplitude further increases the resulting instability amplitude increases; this was clearly explained in Joslin *et al* (1995) to occur because in the wave superposition process, the actuator wave becomes dominant over the forced wave. At this point, the resulting instability undergoes a phase shift corresponding to the phase of the wave generated by the actuator. The relationship depicted in Figure 12 is encouraging for the DNS/optimal control theory approach and suggests that a gradient descent type algorithm might further enhance the wave suppression capability of the present approach. Namely, an approach for the optimal selection of α_1, α_2, β_1, and β_2 might lead to a more useful theoretical/computational tool for flow control.

To simply demonstrate this concept, Lagrange interpolation (or perhaps extrapola-

tion) is introduced for β_1 and β_2 based on imposed values for α_1 and α_2:

$$\beta_{1,2}^{n+1} = \frac{\beta_{1,2}^{n}(\tau_{1,2}^{*} - \tau_{1,2}^{n-1}) - \beta_{1,2}^{n-1}(\tau_{1,2}^{*} - \tau_{1,2}^{n})}{(\tau_{1,2}^{n} - \tau_{1,2}^{n-1})}, \tag{55}$$

where $\tau_{1,2}^{*}$ are some desired values of the stress components and $\tau_{1,2}^{n}$ are the stress components based on the choice $\beta_{1,2}^{n}$. Although τ_1^* and τ_2^* may be equivalent to the target values τ_1 and τ_2 in the functional (11), this may lead to significant over/under shoots for the interation process. Instead, τ_1^* and τ_2^* is the incremental decrease, or target value, for interpolation to more desirable β_1 and β_2 values. To illustrate this process, the $\beta_2 = 10$ (C2) and $\beta_2 = 11$ control results are obtained with the iteration procedure. The measures of normal stress are somewhat arbitrarly obtained at some time as measured by the sensor or matching segment Γ_s; the values of the normal stress are given in the Table 1. These values are used for a desired normal stress τ_2^*, which in this case is 65% of the $\beta_2 = 11$ results.

β_2	normal stress
10	9.369×10^{-6}
11	8.814×10^{-6}

Table 1. Normal stress for two values of β_2.

Using the results for $\beta_2 = 10$ and $\beta_2 = 11$ in (55) yields the value $\beta_2 = 16.5$ which is used in a simulation to obtain a greater degree of instability suppression. The WC results and the enhanced optimal control (C3) solution are shown in Figures 13 and 14. This interpolation approach based on relationship of Figure 12 indicates that optimizing β_2 has led to results very close to WC. The solutions differ somewhat near $t = T_a$ and $t = T_b$ because of the conditions (48) and (50) that serve to control the levels of g_1 and g_2. For all practical purposes, the solutions obtained with the present DNS/control theory methodology yield the desired flow control features without prior knowledge of the forced instability.

The adjoint system requires that the velocity field (u, v) obtained from the Navier-Stokes equations (34)-(40) be known for all time. For the iteration sequence and a modestly course grid, 82 Mbytes of disk (or runtime) space are required to store the velocities at all time steps and for all grid points. For $T_a \rightarrow T_b = 3T_p$, 246 Mbytes are necessary for the computation. Clearly for three-dimensional problems the control scheme becomes prohibitively expensive. Therefore, a secondary goal of this study is to determine if this limitation can be elliminated.

Because the characteristics of the actuator (g_1 and g_2) and resulting solutions are comparable to WC, some focus should be placed on elliminating the enormous memory requirements discussed above. This limitation can easily be removed if the flow-control problem involves small-amplitude unsteadiness (or instabilities). The time-dependent coefficients of the adjoint system (41)-(42) reduce to the steady-state solution and no addition memory is required over the Navier-Stokes system in terms of coefficients. This has been verified by a comparison of a simulation with steady coefficients compared with the C2 control case. The results shown in Figure 15 are identical (as expected). Additionally, if the instabilities have small amplitudes, then a linear Navier-Stokes solver can be used instead of the full nonlinear solver, which was used in the present study. This linear system would be very useful for the design of flow-control systems. However, if the instabilities in the flow have sufficient amplitude to interact nonlinearly, then some measure of unsteady coefficient behavier is likely required. Depending on the amplitudes, the coefficients saved at every time-step may be replaced with storing coefficients every 10 or more time-steps thereby reducing the memory requirements by an order of magnitude. This hypothesis will require validation in a future study.

CONCLUSIONS

The coupled Navier-Stokes equations, adjoint Navier-Stokes, and optimality condition equations were solved and validated for the flow-control problem of instability wave suppression in a two-dimensional, flat plate, boundary layer. By solving the above system, optimal controls were determined that met the objective of minimizing the perturbation normal stress along a portion of the bounding wall. As a result, the optimal control was found to be an effective means for suppressing two-dimensional, unstable Tollmien-Schlichting travelling waves. The results indicate that the DNS/control theory solution is comparable to the wave-cancellation result but, unlike the latter, requires no a priori knowledge of the instability characteristics.

ACKNOWLEDGEMENTS

Max Gunzburger was also supported by the Air Force Office of Scientific Research under grant number AFOSR-93-1-0280.

REFERENCES

BIRINGEN, S. 1984 Active control of transition by periodic suction-blowing. *Phys. Fluids*, **27**(6), 1345-1347.

BORGGAARD, J., BURKARDT, J., GUNZBURGER, M. & PETERSON, J. 1995 *Optimal Design and Control*, Birkhauser, Boston.

BOWER, W. W., KEGELMAN, J. T., PAL, A. & MEYER, G. H. 1987 A numerical study of two-dimensional instability-wave control based on the Orr-Sommerfeld equation. *Phys. Fluids* **30**(4), 998-1004.

BUTTER, D. J. 1984 Recent progress on development and understanding of high-lift systems. AGARD-CP-365.

COUSTEIX, J. 1992 Basic concepts on boundary layers. AGARD-R-786.

DANABASOGLU, G., BIRINGEN, S. & STREETT, C. L. 1991 Spatial simulation of instability control by periodic suction and blowing. *Phys. Fluids* A **3**(9), 2138-2147.

FURSIKOV, A. V., GUNZBURGER, M. & HOU, L. 1995 Boundary value problems and optimal boundary control of the Navier-Stokes system: The two-dimensional case, to appear in *SIAM J. Cont. Optim.*.

GAD-EL-HAK, M. 1989 Flow control. *Appl. Mech. Rev.* **42**(10), 261-293.

GAD-EL-HAK, M. and BUSHNELL, D. M. 1991 Separation control: review. *J. Fluids Engineering*, **113**, 5-30.

GAD-EL-HAK, M. 1994 Interactive control of turbulent boundary layers: A futuristic overview. *AIAA J.* **32**(9), 1753-1765.

GUNZBURGER, M. 1995 *Flow Control*, Springer, Berlin.

JOSLIN, R. D., STREETT, C. L. & CHANG C.-L. 1992 Validation of three-dimensional incompressible spatial direct numerical simulation code – a comparison with linear stability and parabolic stability equations theories for boundary-layer transition on a flat plate. NASA TP-3205.

JOSLIN, R. D., STREETT, C. L. & CHANG, C.-L. 1993 Spatial direct numerical simulation of boundary-layer transition mechanisms: Validation of PSE theory. *Theor. Comput. Fluid Dyn.* **4**, 271-288.

JOSLIN, R. D., ERLEBACHER, G. & HUSSAINI, M. Y. 1995 Active control of instabilities in laminar boundary-layer flow. An overview. to appear in *J. Fluids Eng.*. (Also appeared as NASA-CR 195016, ICASE Report No. 94-97.)

KEEFE, L. R. 1993 Drag reduction in channel flow using nonlinear control. AIAA Paper No. 93-3279.

KRAL, L. D. & FASEL, H. F. 1989 Numerical investigation of the control of the secondary instability process in boundary layers. AIAA Paper 89-0984.

LADD, D. M. & HENDRICKS, E. W. 1988 Active control of 2-D instability waves on an axisymmetric body. *Experiments in Fluids* **6**, 69-70.

LADD, D. M. 1990 Control of natural laminar instability waves on an axisymmetric body. *AIAA J.* **28**(2), 367-369.

LAURIEN, E. & KLEISER, L. 1989 Numerical simulation of boundary-layer transition and transition control. *J. Fluid Mech.* **199**, 403-440.

LIEPMANN, H. W. & NOSENCHUCK, D. M. 1982 Control of laminar-instability waves using a new technique. *J. Fluid Mech.* **118**, 187-200.

LIEPMANN, H. W. & NOSENCHUCK, D. M. 1982 Active control of laminar-turbulent transition. *J. Fluid Mech.* **118**, 201-204.

MAESTRELLO, L. & TING, L. 1984 Analysis of active control by surface heating. AIAA Paper 84-0173.

METCALFE, R. W., RUTLAND, C., DUNCAN, J. H. & RILEY, J. J. 1985 Numerical simulations of active stabilization of laminar boundary layers. AIAA Paper 85-0567.

MILLING, R. W. 1981 Tollmien-Schlichting wave cancellation. *Phys. Fluids* **24**(5), 979-981.

MUIRHEAD, V. U. 1978 An investigation of drag reduction for tractor-trailer vehicles. NASA CR 144877.

OTT, E. A., GREBOGI, C. & YORKE, J. A. 1990 Controlling chaos. *Phys. Rev. Lett.* **64**(11), 1196.

PAL, A., BOWER, W. W. & MEYER, G. H. 1991 Numerical simulations of multifrequency instability-wave growth and suppression in the Blasius boundary layer. *Phys. Fluids* A **3**(2), 328-340.

PUPATOR, P. & SARIC, W. 1989 Control of random disturbances in a boundary layer. AIAA Paper 89-1007.

STREETT, C. L. & HUSSAINI, M. Y. 1991 A numerical simulation of the appearance of chaos in finite-length Taylor-Couette flow. *Appl. Numer. Math.* **7**, 41-71.

STREETT, C. L. & MACARAEG, M. G. 1989 Spectral multi-domain for large-scale fluid dynamics simulations. *Appl. Numer. Math.* **6**, 123-140.

THOMAS, A. S. W. 1983 The control of boundary-layer transition using a wave-superposition principle. *J. Fluid Mech.* **137**, 233-250.

WILKINSON, S. P. 1989 Interactive wall turbulence control. *Viscous Drag Reduction in Boundary Layers* (eds. D.M.Bushnell and J.N.Hefner), Progress in Astronautics and Aeronautics, **123**, 479-509.

WILLIAMSON, J. H. 1980 Low-storage Runge-Kutta schemes. *J. Comput. Phys.* **35**(1), 48-56.

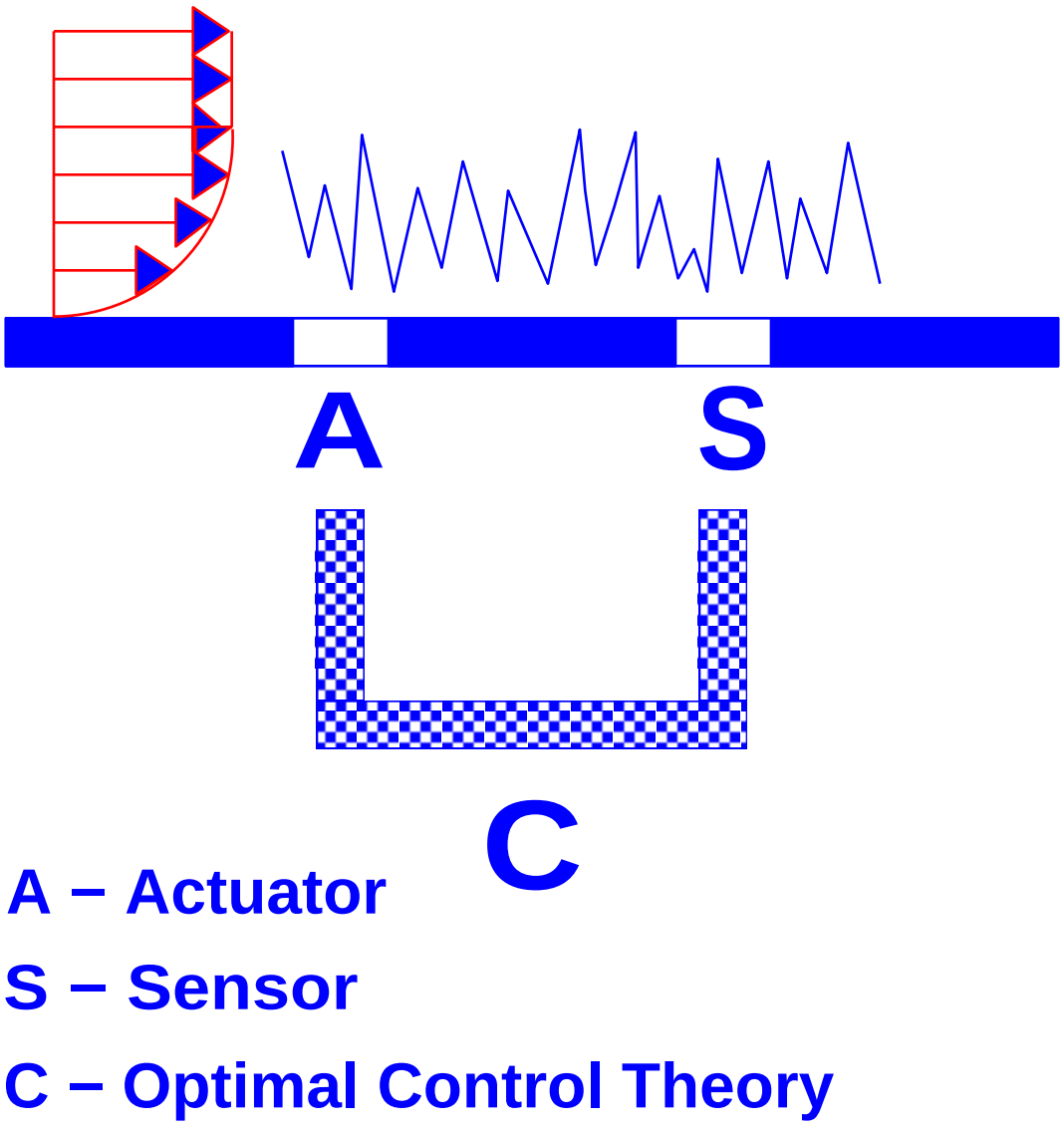

Figure 1. Schematic of active flow control using optimal control theory.

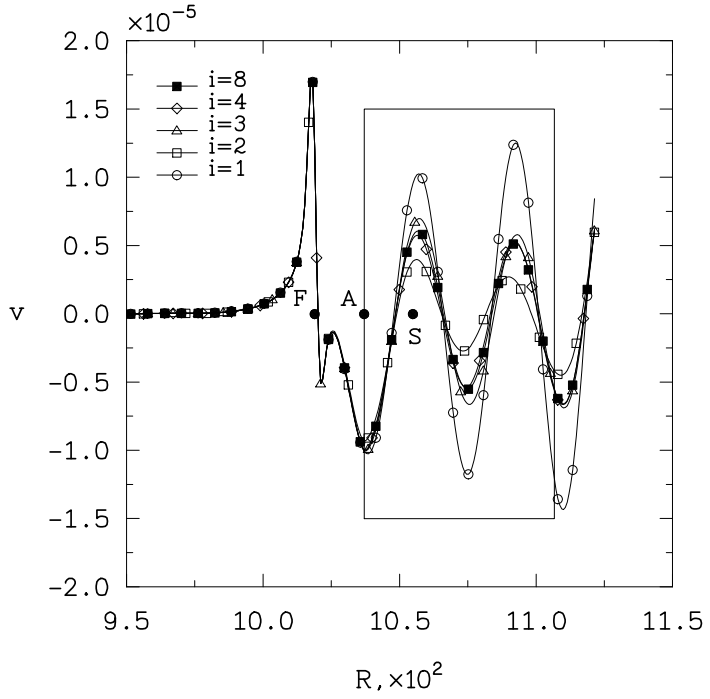

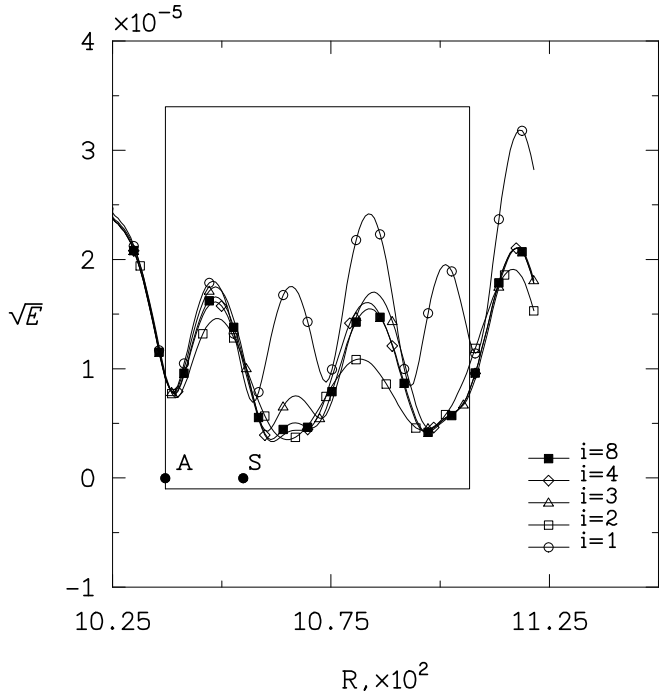

Figure 2. Convergence of disturbance wall-normal velocity and energy with downstream distance for control in flat-plate boundary-layer flow. (Velocity signal at $y = 1.18\delta_o^*$ from wall; $T_1 - T_0 = 2T_p$.)

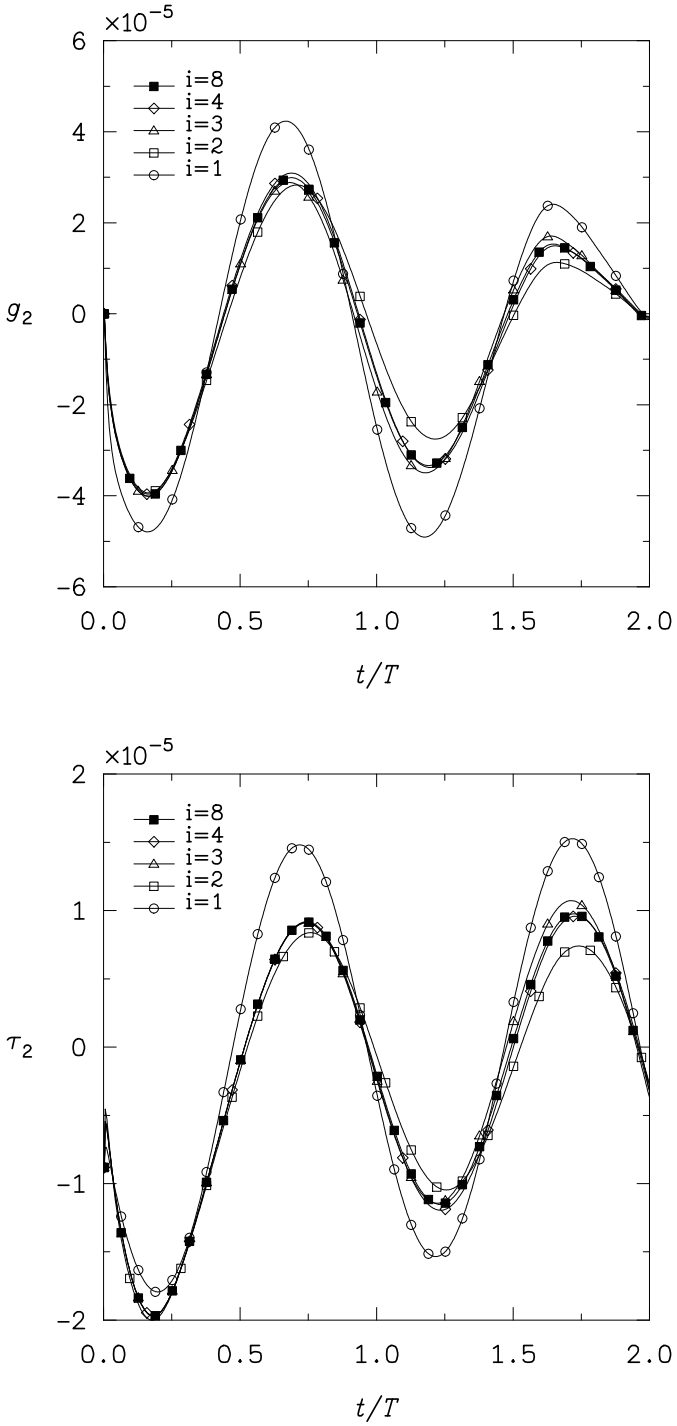

Figure 3. Convergence of actuator response and sensor-measured shear stress with discrete time.

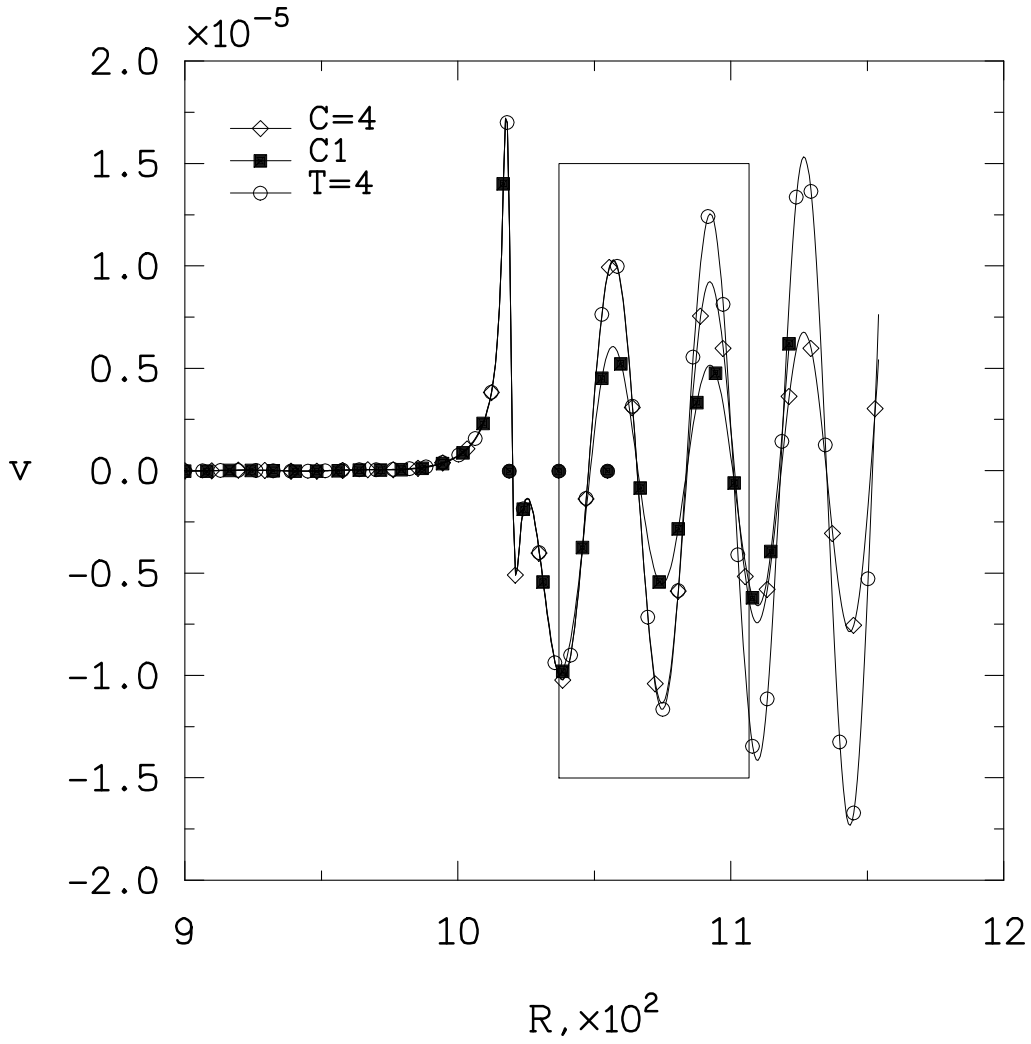

Figure 4. Disturbance velocities with downstream distance for no control (T=4), control (C1), and after control is used and turned-off (C=4) in flat-plate boundary-layer flow. (Velocity signal at y=1.18δ_o^* from wall.)

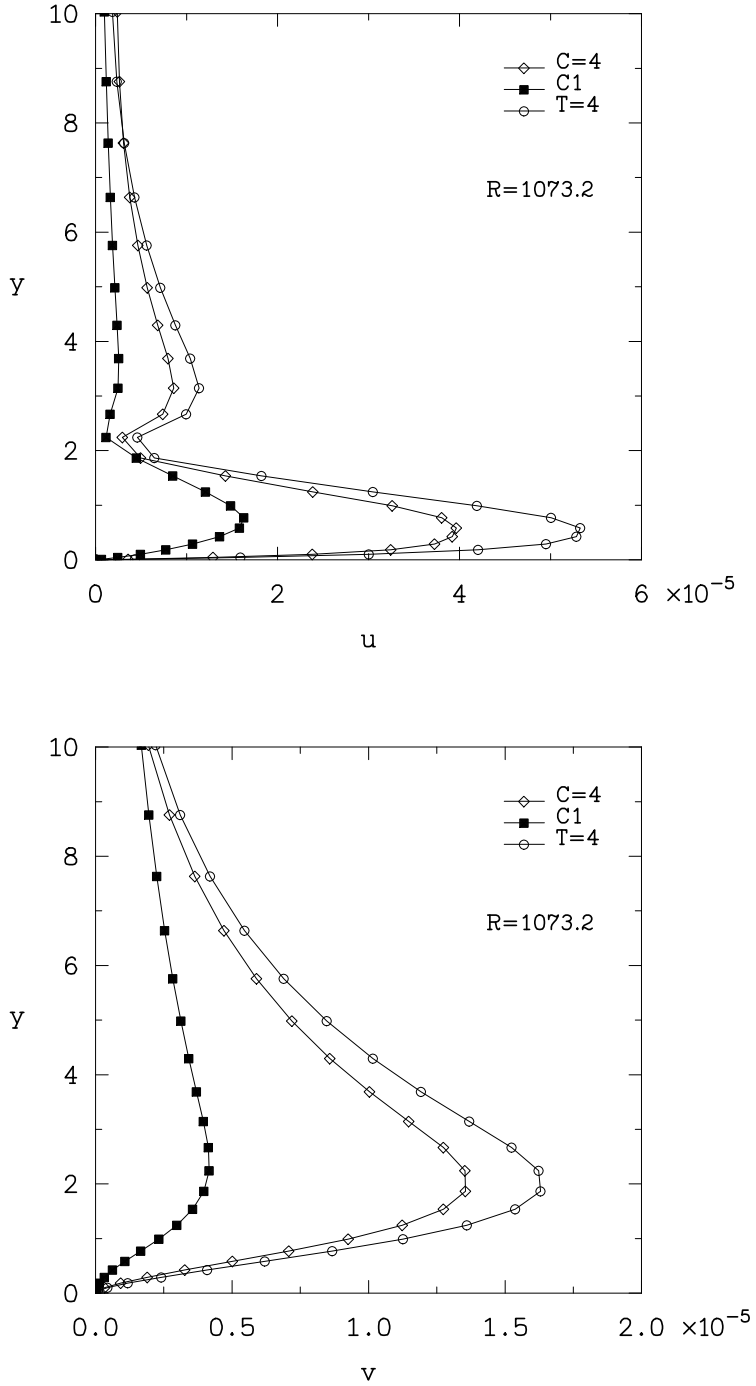

Figure 5. Disturbance velocity profiles for no control (T=4), contro l(C1), and after control is used and turned-off (C=4) in flat-plate boundary-layer flow.

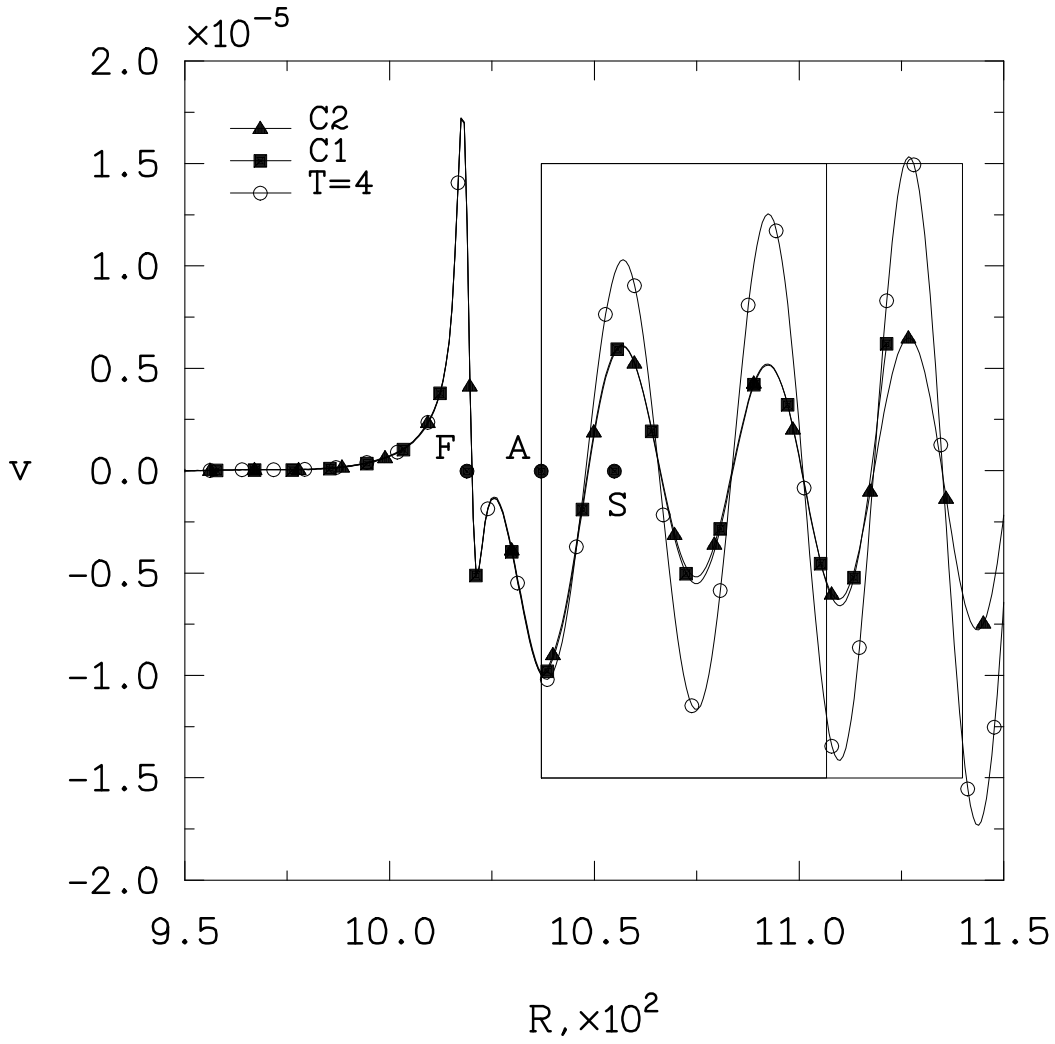

Figure 6. Disturbance velocity with downstream distance for no control (T=4) and control (C1 for $T_1 - T_0 = 2T_p$ and C2 for $T_1 - T_0 = 3T_p$) in flat-plate boundary-layer flow. (Velocity signal at $y = 1.18\delta_o^*$ from wall.)

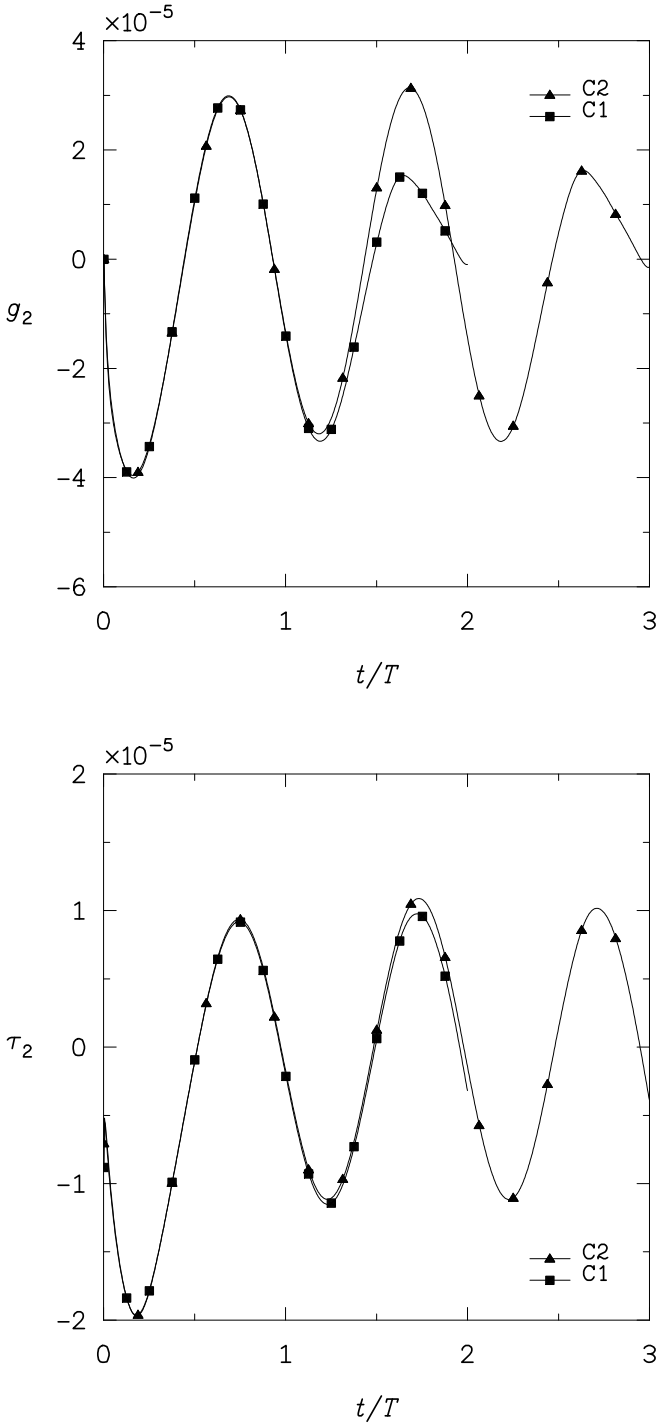

Figure 7. Actuator response and sensor-measured shear stress for controls (C1 for $T_1 - T_0 = 2T_p$ and C2 for $T_1 - T_0 = 3T_p$) with discrete time.

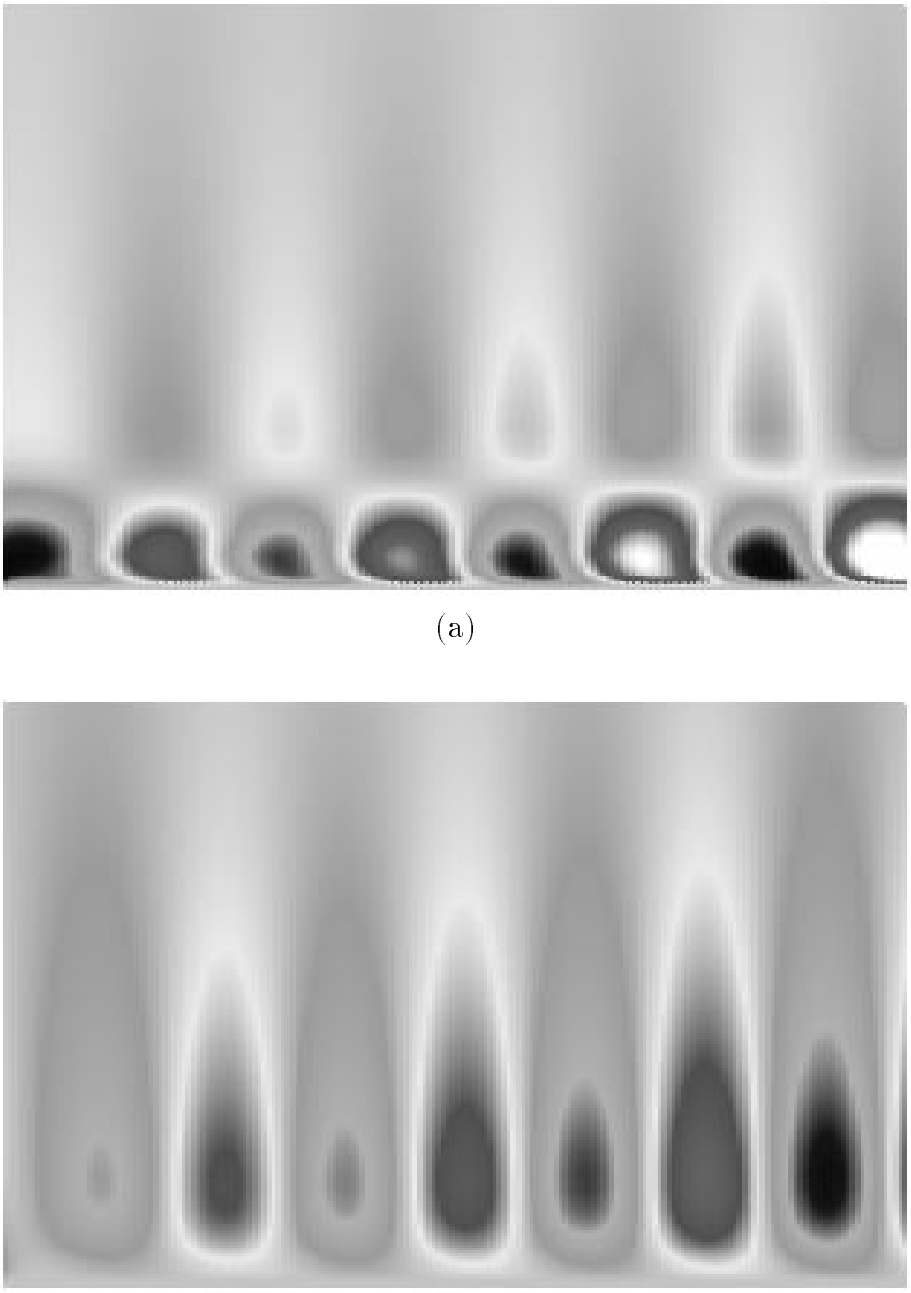

(a)

(b)

Figure 8. Contours of (a) u and (b) v velocities for no control in flat-plate boundary-layer flow. (Contours: 7.5×10^{-5} to -7.5×10^{-5}; intensity increases left-to-right)

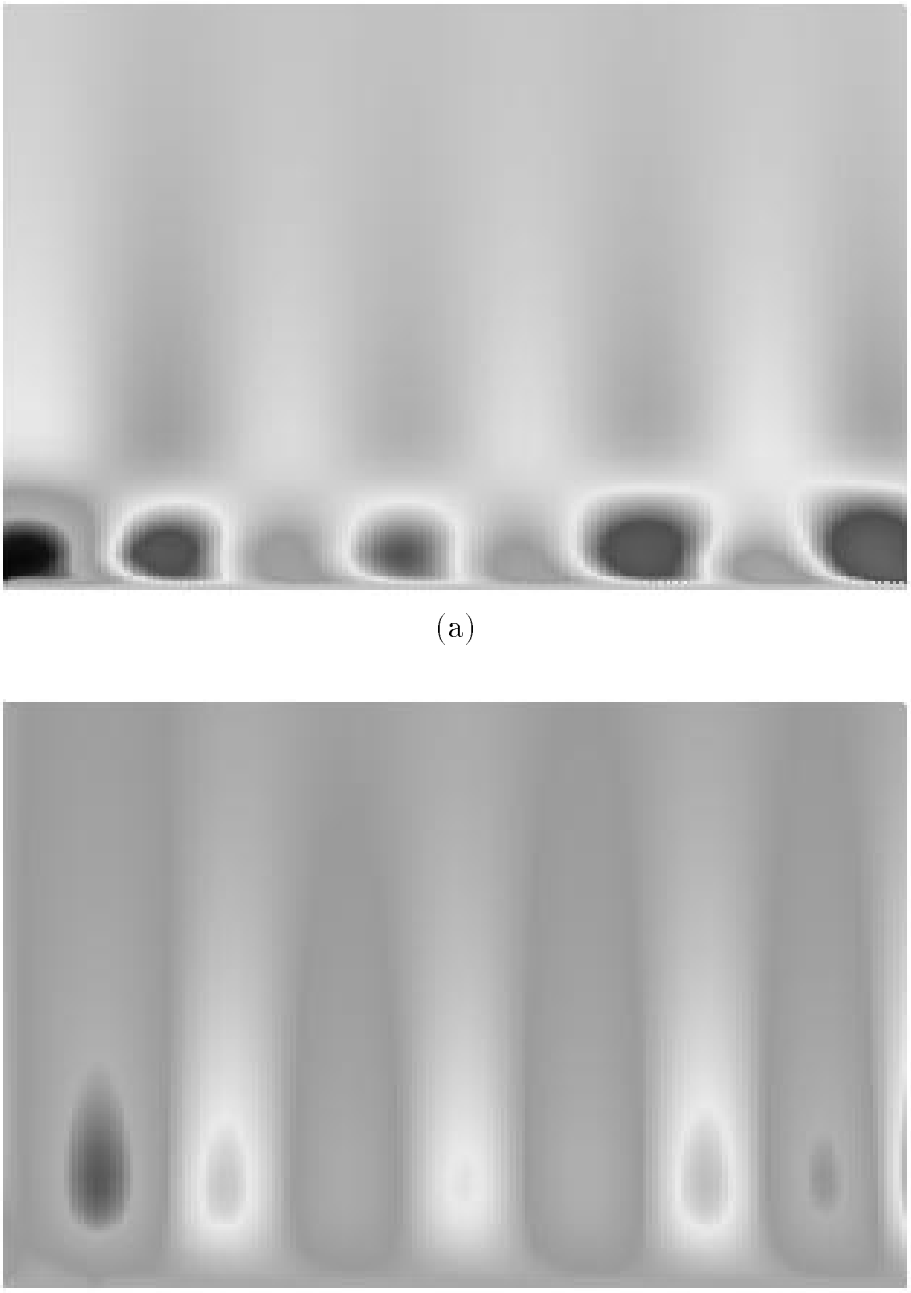

(a)

(b)

Figure 9. Contours of (a) u and (b) v velocities for control in flat-plate boundary-layer flow. (Contours: 7.5×10^{-5} to -7.5×10^{-5}.)

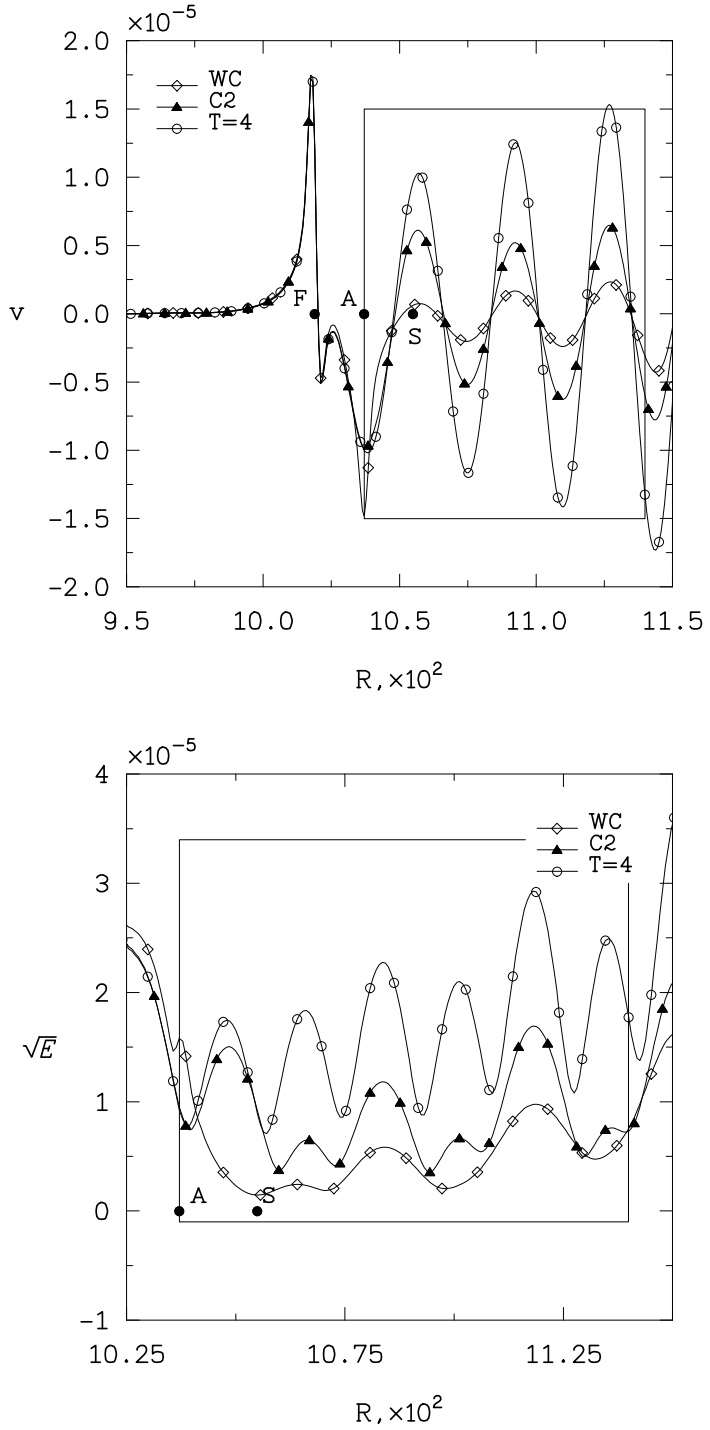

Figure 10. Disturbance velocity and energy with downstream distance for no control (T=4), control (C2), and wave cancellation (WC) in flat-plate boundary-layer flow. (Velocity signal at $y = 1.18\delta_o^*$ from wall; $T_1 - T_0 = 3T_p$.)

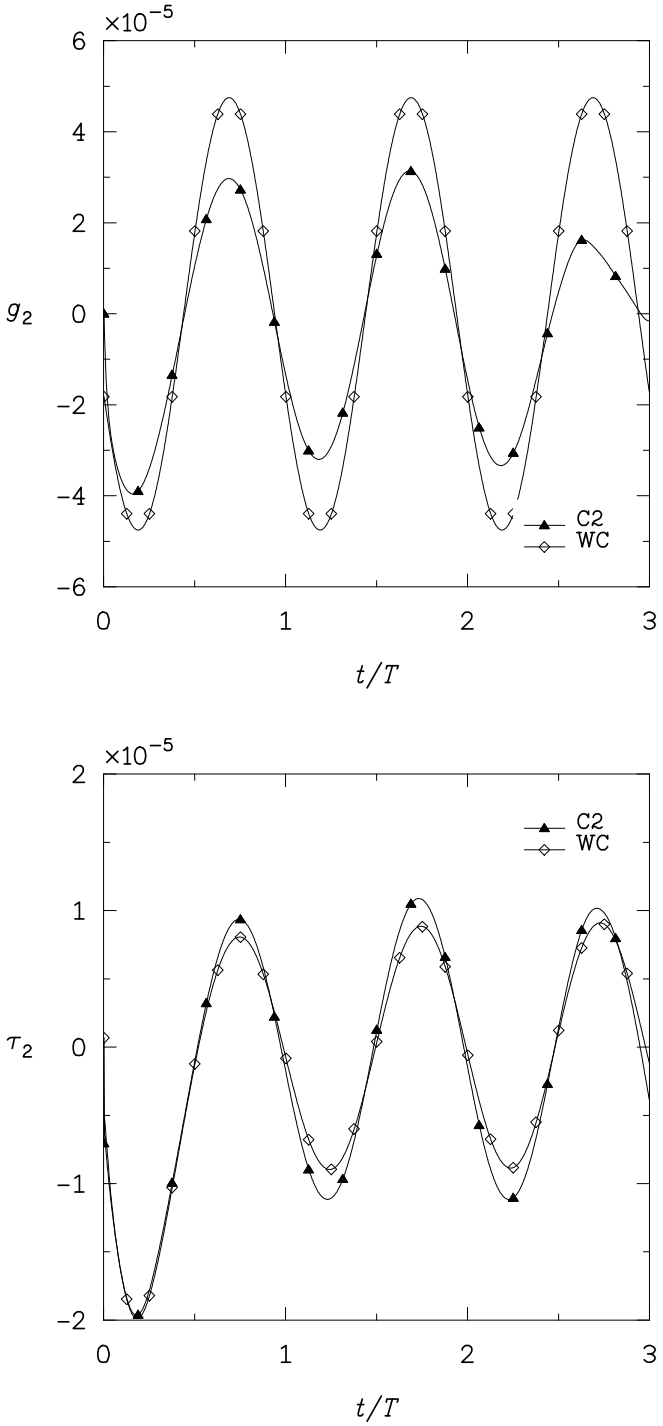

Figure 11. Actuator response and sensor-measured shear stress for control (C2) and wave cancellation (WC) with discrete time.

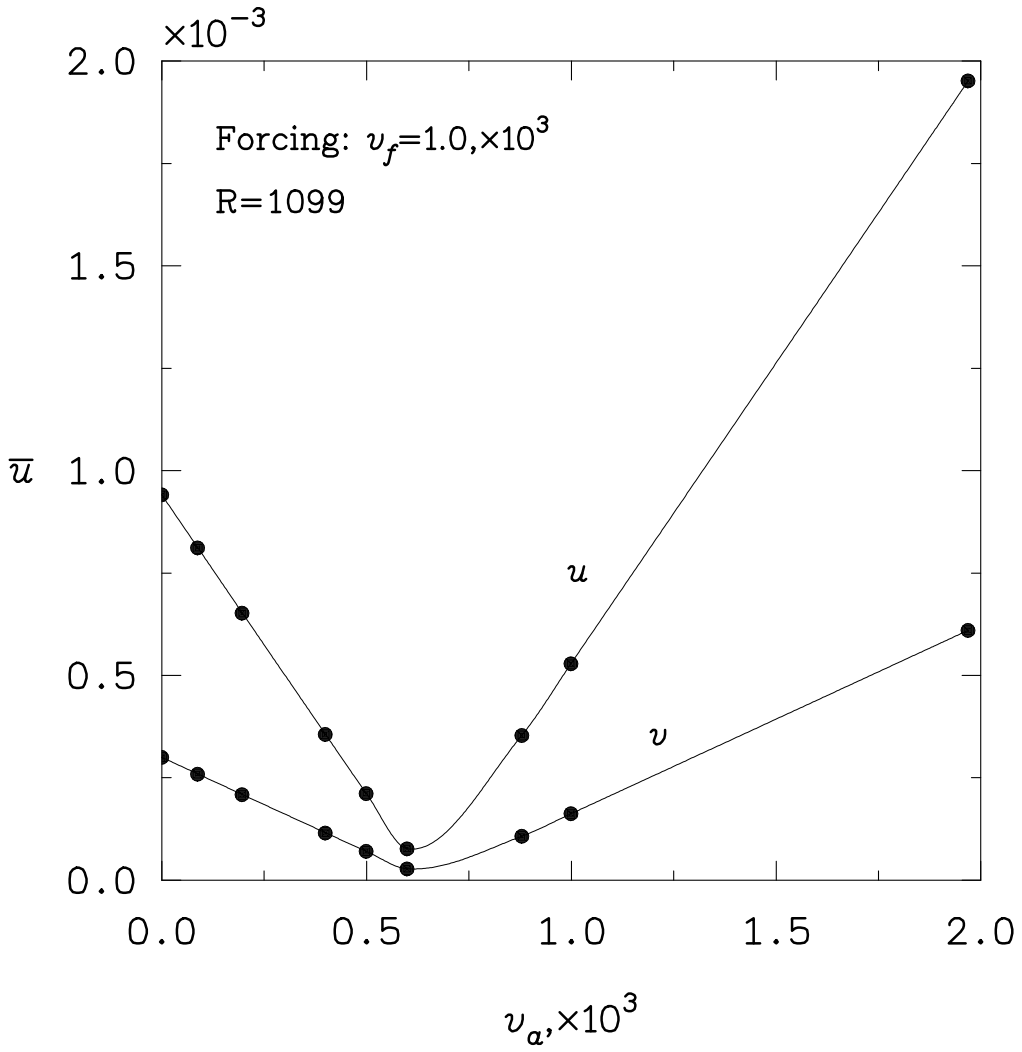

Figure 12. Disturbance velocity resulting from variations in actuator amplitude from simulations in Joslin *et al* (1995).

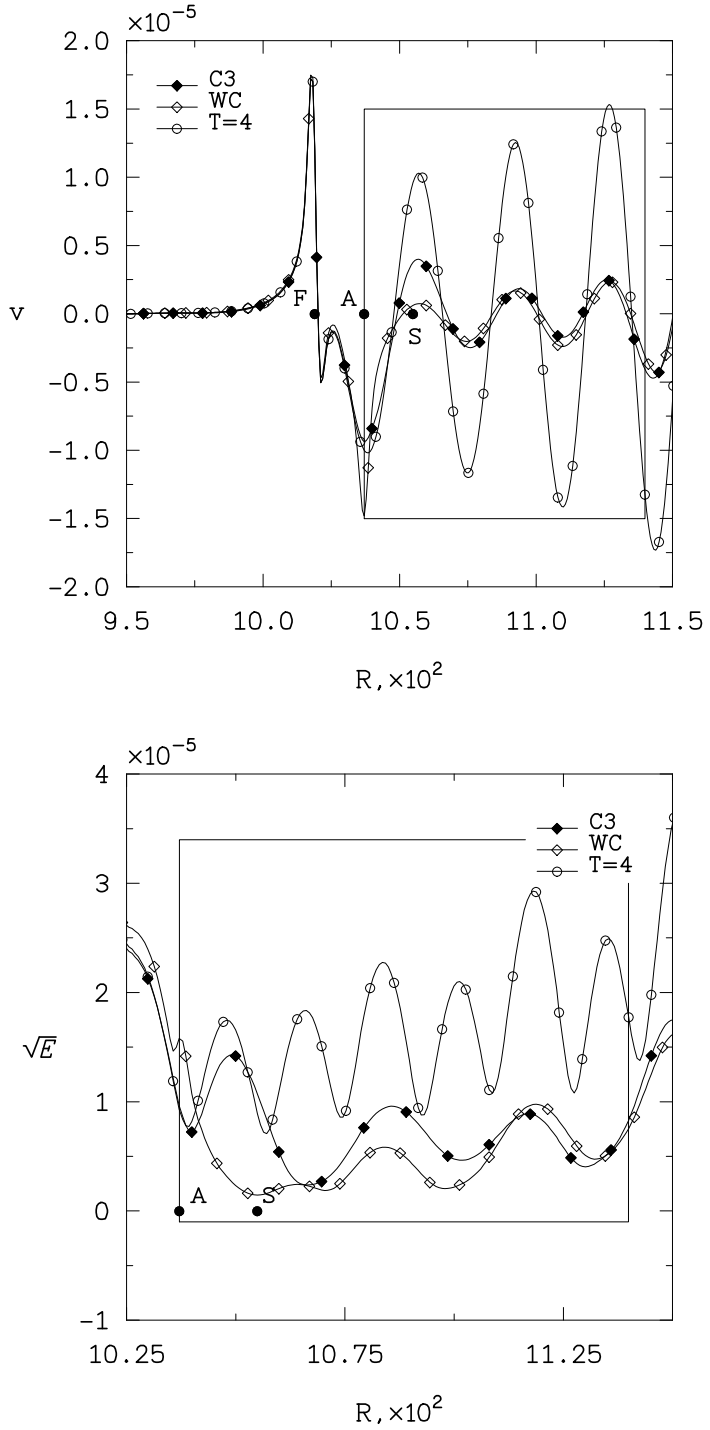

Figure 13. Disturbance velocity and energy with downstream distance for no control (T=4), control (C2), control (C3), and wave cancellation (WC) in flat-plate boundary-layer flow. (Velocity signal at $y = 1.18\delta_o^*$ from wall; $T_1 - T_0 = 3T_p$.)

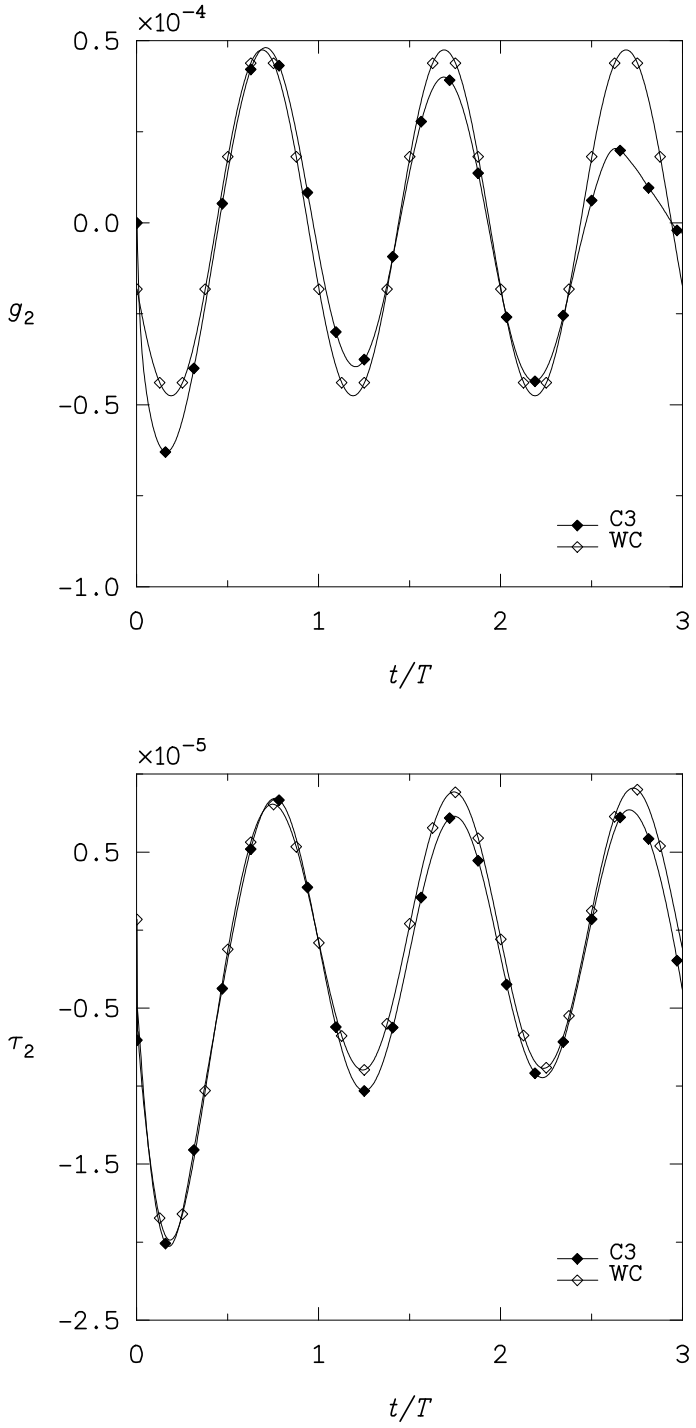

Figure 14. Actuator response and sensor-measured shear stress for control (C2), control (C3), and wave cancellation (WC) with discrete time.

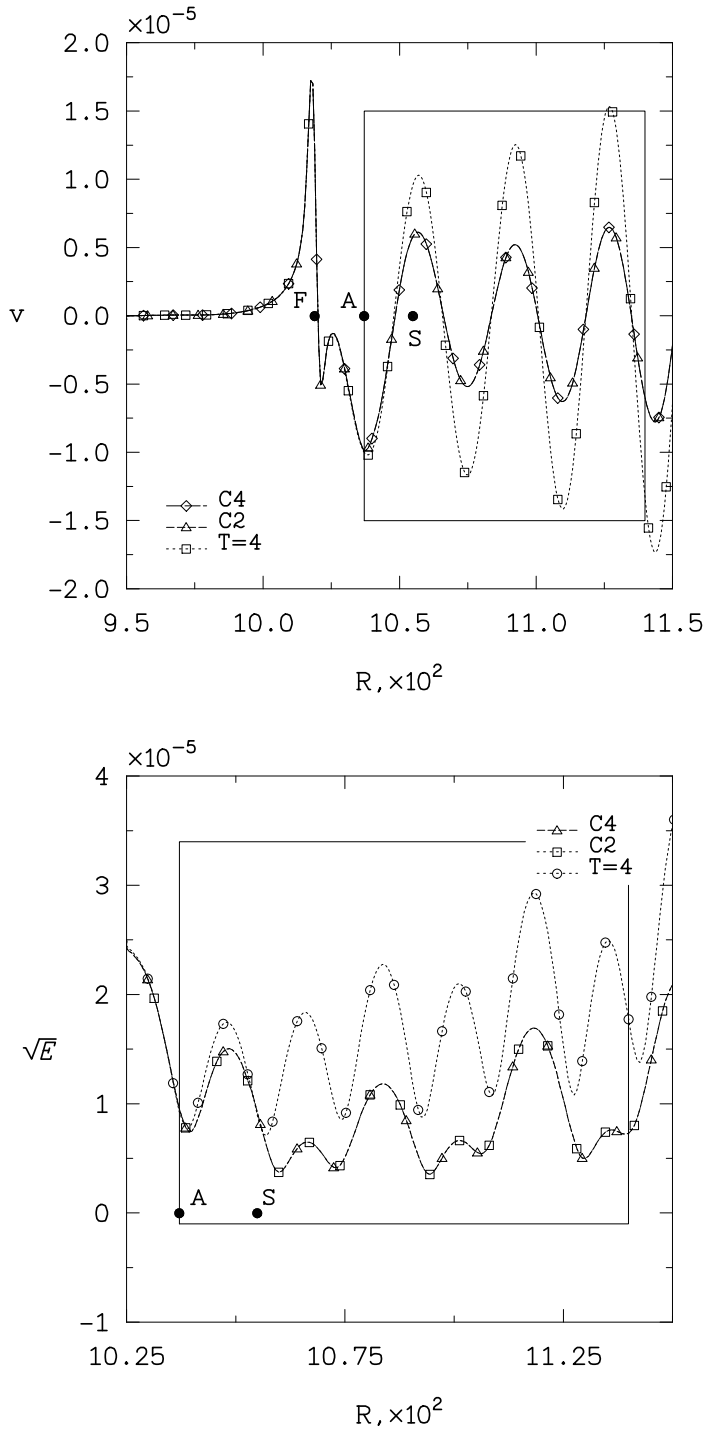

Figure 15. Disturbance velocity and energy with downstream distance for no control (T=4), control (C2), and control (C4-steady coefficients) in flat-plate boundary-layer flow. (Velocity signal at $y = 1.18\delta_o^*$ from wall; $T_1 - T_0 = 3T_p$.)